

C IV Emission-line Properties and Uncertainties in Black Hole Mass Estimates of $z\sim 3.5$ Ouasars

Wenwen Zuo¹, Xue-Bing Wu^{2,3}, Xiaohui Fan⁴, Richard Green⁴, Weimin Yi^{5,6}, Andreas Schulze⁷, Ran Wang³, and Fuyan Bian⁸

Shanghai Astronomical Observatory, Chinese Academy of Sciences, 80 Nandan Road, Shanghai 200030, People's Republic of China; wenwenzuo@shao.ac.cn Department of Astronomy, School of Physics, Peking University, Beijing 100871, People's Republic of China Kavli Institute for Astronomy and Astrophysics, Peking University, Beijing 100871, People's Republic of China

Steward Observatory, The University of Arizona, Tucson, AZ 85721, USA
 Yunnan Observatories, Kunming, 650216, People's Republic of China

⁶ Key Laboratory for the Structure and Evolution of Celestial Objects, Chinese Academy of Sciences, Kumming 650216, People's Republic of China National Astronomical Observatory of Japan, Mitaka, Tokyo 181-8588, Japan

European Southern Observatory, Alonso de Córdova 3107, Casilla 19001, Vitacura, Santiago 19, Chile Received 2019 November 8; revised 2020 May 5; accepted 2020 May 8; published 2020 June 11

Abstract

Using a high-luminosity ($L_{\rm bol} \sim 10^{47.5}$ – $10^{48.3}$ erg s⁻¹), high-redshift (3.2 < z < 3.8) quasar sample of 19 quasars with optical and near-infrared spectroscopy, we investigate the reliability of the C IV-based black hole mass estimates ($M_{\rm BH}$). The median logarithm of the C IV- and H β -based $M_{\rm BH}$ ratios is 0.110 dex, with a scatter of 0.647 dex. The C IV-to-H β BH mass differences are significantly correlated with the C IV FWHMs, blueshifts, and asymmetries. Corrections of the C IV FWHM using the blueshift and asymmetry reduce the scatter of the mass differences by ~0.04–0.2 dex. Quasars in our sample accrete at the Eddington ratio $R_{\rm EDD} > 0.3$ and cover a considerable range of blueshifts, with 18/19 of the quasars showing C IV blueshifts (with the median value of 1126 km s⁻¹) and 14/19 of the quasars showing C IV blueshifts larger than 500 km s⁻¹. It suggests that not all quasars with high Eddington ratios show large blueshifts. The Baldwin effect between the C IV rest-frame equivalent width (REW) and the continuum luminosity at 1350 Å is not seen, likely due to the limited luminosity range of our sample. We find a lack of flux in the red wing of the composite spectrum with larger C IV blueshift and detect a higher ratio of [O III] quasars with REW_[O III] > 5 Å in the subsample with lower C IV blueshift. It is more likely that they are caused by the combination of the Eddington ratio and the orientation effect.

Unified Astronomy Thesaurus concepts: Black hole physics (159); Quasars (1319)

1. Introduction

It is commonly accepted that black holes (BHs) reside in the center of massive galaxies, and the BH mass ($M_{\rm BH}$) tightly correlates with properties of the host galaxy, i.e., the mass of the host galaxy spheroidal component and its velocity dispersion (Ferrarese & Merritt 2000; Gebhardt et al. 2000; Tremaine et al. 2002; Gültekin et al. 2009; Graham et al. 2011; Kormendy & Ho 2013). These scaling relations strongly suggest that BH growth is coupled with galaxy mass assembly history (Nelson et al. 2004; Onken et al. 2004; Kormendy & Ho 2013). To understand the growth history of BHs and the connection between the BH and the host galaxy, it is important to obtain reliable BH mass estimates.

Assuming that the line-emitting clouds in the broad-line region (BLR) are virialized under the gravity of the central BH, the BH mass can be estimated with the BLR size and the virial velocity of the BLR clouds. The FWHM or the dispersion of the broad emission line is commonly used to represent the virial velocity. Mainly for low-redshift active galactic nuclei (AGNs), the reverberation mapping (RM) technique has been applied; the time lag of the variations between the broad emission line and the continuum luminosity is used to trace the typical BLR size (Peterson 1993; Peterson et al. 2004).

However, the RM technique requires long-term observational campaigns and is especially challenging at higher redshift (Kaspi et al. 2000, 2007; Peterson et al. 2004; Bentz et al. 2009; Denney et al. 2010; Du et al. 2014; Barth et al. 2015; Shen et al. 2015; Grier et al. 2017, 2019). A tight

correlation between the BLR size (*R*) and the quasar continuum luminosity in optical bands has been revealed from the RM campaigns (Kaspi et al. 2000, 2005; Bentz et al. 2013). This relation provides an alternative inexpensive way to estimate the BLR size through single-epoch (SE) spectroscopy, further leading to the so-called SE virial BH mass estimates.

Under the virial assumption, BH masses for a large sample of AGNs can be calculated with the product of the BLR size and the virial velocity based on the SE spectroscopy via $M_{\rm BH} \propto R \times v^2$, with coefficients fairly well calibrated from 40 z < 0.7 AGNs with H β -based RM $M_{\rm BH}$ (Kaspi et al. 2000; Peterson et al. 2004). Typically, in the SE method the H β broad emission line width and the continuum luminosity at 5100 Å are used (e.g., Greene & Ho 2005; Vestergaard & Peterson 2006; McGill et al. 2008; Shen et al. 2011; Shen & Liu 2012; Shen 2013; Zuo et al. 2015; Coatman et al. 2017; Schulze et al. 2018; Coffey et al. 2019; Marziani et al. 2019).

At redshift larger than 2, both the H β line and the Mg II line have moved out of the optical observing window. Such SE estimates have been extrapolated to the C IV $\lambda1549$ emission line in the rest-frame ultraviolet wavelength (McLure & Jarvis 2002; Vestergaard 2002; Vestergaard & Peterson 2006; Vestergaard & Osmer 2009; Denney 2012; Park et al. 2013, 2017; Coatman et al. 2016, 2017; Sulentic et al. 2017; Marziani et al. 2019).

However, given the fact that before the Sloan Digital Sky Survey (SDSS) RM project (for a technical overview, see Shen et al. 2015) the RM technique is mainly based on the ${\rm H}\beta$ emission line for the low-redshift AGN sample, the C IV

emission line lacks direct calibrations from large samples. The most recently obtained C IV radius–luminosity relation based on the SDSS-RM project has raised the number of sources from $\sim\!15$ to $\sim\!67$ (Grier et al. 2019). However, it is still controversial whether calibrations based on the overlap of the RM and the SE methods can reliably estimate the C IV-based BH masses for high-redshift luminous quasars (Shen et al. 2008; Shen & Liu 2012; Park et al. 2013).

The C IV emission line is commonly known to show asymmetry and blueshift with respect to the low-ionization lines (Gaskell 1982; Marziani et al. 1996, 2019; Sulentic et al. 2000, 2017; Shen et al. 2008; Richards et al. 2011; Denney 2012; Coatman et al. 2016, 2017; Mejía-Restrepo et al. 2018; Schulze et al. 2018; Vietri et al. 2018; Ge et al. 2019). These features suggest that, compared with the Mg II and H β lines, the C IV line width is probably more affected by a nonvirial velocity component owing to disk winds of ejected materials (Konigl & Kartje 1994; Murray et al. 1995; Proga et al. 2000; Marziani et al. 2010; Richards et al. 2011).

It is therefore essential to consider the effects of these features on the $M_{\rm BH}$ estimates. One straightforward approach to test the reliability of the C IV-based BH mass estimates is the systematic comparison with the Balmer line for the same objects.

Using a sample of 16 lensed quasars, Greene et al. (2010) found no systematic biases in the BH mass estimates between the Balmer lines and the C IV line, although the scatter is large. Based on a sample of 12 quasars, Assef et al. (2011) found no systematic offsets between the C IV and Balmer line mass estimates, but they did see that the differences between BH mass estimates strongly correlate with the logarithm of the ratios of the UV and optical continuum luminosities.

Based on 60 luminous quasars, Shen & Liu (2012) found that the C IV line can be calibrated to yield consistent BH mass estimates with those based on the H β line, but the scatter is substantially larger than Mg II. They concluded that the line width of Mg II correlates well with that of H β from the SE spectroscopy, while the C IV line width is poorly correlated with the Mg II or H β line widths. Some other studies suggested that poor correlations between different line widths play more important roles than the continuum luminosities in the differences of virial BH mass estimates (Shen et al. 2008; Denney 2012; Trakhtenbrot & Netzer 2012; Park et al. 2013, 2017; Runnoe et al. 2013; Coatman et al. 2017; Sulentic et al. 2017; Mejía-Restrepo et al. 2018; Marziani et al. 2019).

Based on a sample of high-z luminous quasars with 0.9 < z < 3.1 and $10^{47.4}$ erg s⁻¹ $< L_{\rm bol} < 10^{48.4}$ erg s⁻¹, Sulentic et al. (2017) confirmed that for high-luminosity quasars with strong C IV outflows the full C IV profile cannot perform as a useful virial BH mass estimator for most quasars. By studying the C IV and Balmer lines of 230 luminous quasars with 1.5 < z < 4.0 and $10^{45.5}$ erg s⁻¹ $< L_{\rm bol} < 10^{48}$ erg s⁻¹, Coatman et al. (2017) found that with the increase of the C IV line blueshifts, the scatter of the C IV-based BH mass estimates increases dramatically compared to the Balmer line-based BH masses, with ~ 1 dex at the blueshift larger than 5000 km s⁻¹ and ~ 0.6 dex at the blueshift around $3000 \, {\rm km \, s^{-1}}$. With a sample of quasars with $10^{44} \, {\rm erg \, s^{-1}} < L_{\rm bol} < 10^{48.5} \, {\rm erg \, s^{-1}}$ and 0 < z < 3, Marziani et al. (2019) proposed a scaling law for obtaining the C IV-based BH masses with the corrected FWHM of the C IV line. The correction to the C IV FWHM

depends on the C IV blueshift and the UV luminosity and is related to the quasar main sequence (MS).

Marziani et al. (2019) proposed to compare the C IV and H β profiles along the quasar MS. In the "Eigenvector 1" (EV1) parameter space, the FWHMs of the H β broad component (BC) and the rest-frame equivalent width (REW) ratios of the Fe II λ 4570 blend to the H β BC ($R_{\rm Fe~II}$) are not randomly distributed but instead define a quasar MS (Boroson & Green 1992; Sulentic et al. 2000, 2007, 2017; Marziani et al. 2001, 2003; Shen & Ho 2014). Along with the FWHM of the H β BC and $R_{\rm Fe~II}$, the C IV blueshift as one of the other EV1 parameters can be obtained from the rest-frame optical and UV spectra, allowing us to understand the relations with C IV blueshifts in the context of the EV1 plane.

In our previous work, we have presented near-infrared (NIR) observations of the H β and Mg II lines for 32 luminous $z\sim3.5$ quasars with $10^{47.5}$ erg s $^{-1}< L_{\rm bol}< 10^{48.3}$ erg s $^{-1}$ (Zuo et al. 2015). Based on that sample, here we investigate the reliability of the C IV-based BH mass for high-redshift luminous AGNs. Comparison work based on the sample would complement other studies that have proposed empirical corrections to the C IV-based BH masses (Assef et al. 2011; Denney 2012; Shen & Liu 2012; Park et al. 2013; Runnoe et al. 2013; Coatman et al. 2017; Sulentic et al. 2017; Schulze et al. 2018; Marziani et al. 2019).

The dependence of the C IV-based BH mass estimates on the C IV line blueshift and other physical properties will also be investigated here. Previous works reported the presence of large C IV blueshift in quasars with an H β FWHM less than 4000 km s⁻¹ (Bachev et al. 2004; Sulentic et al. 2007; Marziani et al. 2010), while our work would allow us to extend the detection of large C IV blueshift in quasars with large H β FWHM values (Sulentic et al. 2017; Vietri et al. 2018). In addition, the origin of C IV blueshift is assessed using the correlations of blueshift with other quasar properties, such as the line width, REW, radio-loudness, and Eddington ratio ($R_{\rm EDD}$) (Richards et al. 2002, 2011; Sun et al. 2018; Vietri et al. 2018; Marziani et al. 2019).

We describe our sample and spectral measurements in Section 2. The results are delivered in Section 3 and discussed in Section 4. We summarize our main results in Section 5. Throughout the paper, a flat $\Lambda {\rm CDM}$ cosmology with $\Omega_{\Lambda}=0.7$, $\Omega_0=0.3$, and $H_0=70~{\rm km~s^{-1}~Mpc^{-1}}$ is adopted.

2. Data

2.1. Quasar Sample

We selected our targets from the SDSS DR7 quasar catalog (Schneider et al. 2010; Shen et al. 2011) mainly by constraining the redshift and magnitude ranges. To ensure the Mg II and H β lines residing in NIR spectroscopy, redshifts were restricted between 3.2 and 3.8. Certain redshift ranges were also excluded to avoid the H β or Mg II lines accidentally falling in telluric absorption bands. Apparent Vega magnitudes in J and K bands were limited to brighter than 17 and 16 mag, respectively.

With these criteria, we selected 32 targets from the main DR7 quasar catalog. Among the 32 targets, 30 were observed with the TripleSpec instrument mounted on the Hale 200-inch telescope, yielding a continuous spectral coverage of 0.95–2.46 μm simultaneously at a resolution of 2700 (Herter et al. 2008). The remaining two objects were observed with the LUCI 1 NIR instrument (Hill et al. 2012) mounted on the Large

Binocular Telescope (LBT). *J*- and *K*-band spectra were obtained with a resolution of 8460 and 6687, respectively.

The basic data reduction includes flat-field correction, background subtraction, wavelength calibration, one-dimensional spectra extraction, telluric correction, and absolute flux calibration (Cushing et al. 2004; Becker et al. 2009; Bian et al. 2010; Zuo et al. 2015). These reduced spectra were then dereddened for Galactic extinction (Cardelli et al. 1989; Schlegel et al. 1998) and wavelength corrected to the rest frame. We used the H β and [O III] doublets to determine the systemic redshift for each object. The NIR spectra observations and other related details can be found in Zuo et al. (2015).

After excluding six broad absorption line quasars, there are two quasars with NIR spectra labeled as "poor" and three quasars with NIR spectra labeled as "median." Finally, 21 quasars with NIR spectra labeled as "good" are left (Zuo et al. 2015). Among the 21 quasars, there are 20 quasars with full coverage of the H β line, 20 quasars with full coverage of the Mg II line, and 19 quasars with full coverage of the H β line and Mg II line. All of them have good SDSS spectra with full coverage of the C IV line (signal-to-noise ratio [S/N] per spectral resolution elements larger than 10). Thus, these 19 targets are adopted for the following analysis in this work.

The optical spectra are all collected from the SDSS DR14 database. Table 1 lists the number of the SDSS spectroscopic observations for each quasar, the related information from Shen et al. (2011) (SDSS DR7), and the SDSS spectrum with the highest S/N per pixel obtained after the SDSS DR7 (SDSS DR7+). For the 10 quasars with SDSS DR7+ spectra, the mean S/N of the SDSS DR7 spectra and that of SDSS DR7+ spectra are 25.3 and 32.5, respectively. Our analyses are based on the spectrum with the highest S/N for each quasar, i.e., the SDSS DR7 spectra for nine quasars and the SDSS DR7+ spectra for 10 quasars.

2.2. Spectral Measurements

The procedures employed to derive the properties of the emission lines in the NIR spectra (e.g., $H\beta$, [O III], and Mg II) were described in detail in Zuo et al. (2015). The line properties and the continuum luminosities around these emission lines are taken directly from Zuo et al. (2015). Here we briefly review the procedure to measure the NIR spectra and present our new measurements from the optical spectra (particularly the C IV line) in detail.

For each emission line, we locally fit a pseudo-continuum to the continuum-dominated wavelength range around the line. The pseudo-continuum consists of a power-law continuum and Fe II emissions. As mentioned in earlier studies, the contribution from Fe II around the C IV line is quite small (Shen et al. 2011; Trakhtenbrot & Netzer 2012). Considering the difficulty of constraining the Fe II features, including Fe II in the emission-line fitting will introduce extra uncertainties. Therefore, we decide not to include the Fe II features in the C IV line fitting. The power-law continuum fitting windows around the C IV line are generally selected to be [1445, 1465] Å and [1700, 1705] Å. To alleviate the effects of narrow absorption lines, during the pseudo-continuum fitting and subsequent emission-line fitting, we rejected data points that are 5σ below the 20-pixel boxcar-smoothed spectrum.

 Table 1

 Spectra Information from the SDSS DR7 and DR7+

Name (SDSS)	$N_{ m obs}$	S/N	Note
(1)	(2)	(3)	(4)
J011521.20+152453.3	2	23.61	DR7, highest S/N
J014214.75+002324.2	1	20.37	DR7
J015741.57-010629.6	3	19.22	DR7
		22.61	DR7+, highest S/N
J025021.76-075749.9	2	20.62	DR7, highest S/N
J025905.63+001121.9	6	23.79	DR7
		37.03	DR7+, highest S/N
J030341.04-002321.9	4	25.87	DR7
		27.99	DR7+, highest S/N
J030449.85-000813.4	7	29.62	DR7, highest S/N
J075303.34+423130.8	4	32.94	DR7
		40.69	DR7+, highest S/N
J080430.56+542041.1	2	22.62	DR7, highest S/N
J080819.69+373047.3	4	12.55	DR7
		19.35	DR7+, highest S/N
J080956.02+502000.9	3	18.8	DR7
		27.56	DR7+, highest S/N
J081855.77+095848.0	1	20.67	DR7
J090033.50+421547.0	2	40.85	DR7
		47.48	DR7+, highest S/N
J094202.04+042244.5	2	28.96	DR7
		41.07	DR7+, highest S/N
J115954.33+201921.1	1	39.94	DR7
J173352.23+540030.4	4	35.5	DR7
		36.11	DR7+, highest S/N
J213023.61+122252.0	1	21.24	DR7
J224956.08+000218.0	2	14.56	DR7
		24.95	DR7+, highest S/N
J230301.45-093930.7	1	26.33	DR7

Note. Column (1): name of the quasars. Column (2): number of spectra for this quasar in the SDSS DR14 database. Column (3): average S/N per pixel of this spectrum. Column (4): "DR7" means that the row refers to the information of the spectrum used in the SDSS DR7 catalog (Shen et al. 2011); "DR7+" means that the row refers to the information of the spectrum with the highest S/N per pixel after the SDSS DR7.

After subtracting the pseudo-continuum, the emission lines were fitted with multiple Gaussians (for more details, see Shen et al. 2011, 2019; Zuo et al. 2015). In the wavelength range from 4700 to 5100 Å, we fitted the line profiles with five Gaussians: two for the BC of the H β line, one for the narrow component (NC) of the H β line, and two Gaussians for the [O III] $\lambda\lambda 4959$, 5007 doublets. Each Gaussian fitted to the H β BC was generally constrained with the line center offset $(\Delta \log(\lambda_{\rm rf} \ (\rm \mathring{A})))$ less than 0.015 and the FWHM less than $35,250 \,\mathrm{km \, s^{-1}}$. Minor modifications of the fitting parameters were made if necessary. The NC of H β and the [O III] doublets were tied together with the same line center offsets ($\Delta \log(\lambda_{\rm rf})$ (\mathring{A})) < 0.005) from their theoretic values and the same FWHM. The upper FWHM limit of the NC was imposed as $1200 \, \mathrm{km \, s^{-1}}$ (Shen et al. 2011). If needed, we introduced two additional Gaussians with the same FWHM for the extended wings of the [O III] doublets, which were not tied to the NC of $H\beta$ (Vietri et al. 2018). Among the 19 quasars, the [O III] doublets of seven quasars (listed in bold in Table 2) were modeled with two pairs of Gaussians (Zuo et al. 2015).

In the wavelength range from 2700 to 2900 Å, the BC and NC of the Mg II line were modeled with two Gaussians and one Gaussian, respectively. Each Gaussian fitted to the Mg II BC

https://dr14.sdss.org/optical/spectrum/search

Table 2
The Fitting Details of the C IV Emission Line

Name (SDSS)	$\Delta V_0 \mid \text{REW}_0 \mid \text{FWHM}_0$ $(\text{km s}^{-1} \mid \text{Å} \mid \text{km s}^{-1})$	$\Delta V_1 \mid \text{REW}_1 \mid \text{FWHM}_1$ $(\text{km s}^{-1} \mid \text{Å} \mid \text{km s}^{-1})$	$\Delta V_2 \mid \text{REW}_2 \mid \text{FWHM}_2$ $(\text{km s}^{-1} \mid \text{Å} \mid \text{km s}^{-1})$	BC Indexes	$\Delta V \mid \text{REW} \mid \text{FWHM}$ (km s ⁻¹ Å km s ⁻¹)	Model
(1)	(2)	(3)	(4)	(5)	(6)	(7)
J011521.20+152453.3	4324/11/6362	1852/9/4227	3112/7/22831	0,1,2	2433/27/6483	A
J014214.75+002324.2	919/7/3261	1354/16/11486	795/0/6496	0,1,2	962/24/4730	A
J015741.57-010629.6	1425/26/12906	1938/19/4952	781/4/1600	0,1	1918/45/6489	В
J025021.76-075749.9	-125/3/2722	2128/15/8950	-227/1/853	0,1	140/18/6983	В
J025905.63+001121.9	829/28/13567	995/26/4486	-92/10/1600	0,1	957/55/5562	В
J030341.04-002321.9	196/3/2310	1537/17/6233	905/14/15617	0,1,2	511/34/6383	A
J030449.85-000813.4	933/13/11092	422/8/2563	-114/4/1285	0,1	421/21/3261	В
J075303.34+423130.8	421/18/8671	-10/9/2114	194/0/1600	0,1	22/27/2903	В
J080430.56+542041.1	3905/15/9893	-4716/5/15309	984/10/4612	0,1,2	1258/30/7041	A
J080819.69+373047.3	1873/20/5937	-4673/11/21070	421/0/984	0,1	1755/31/6714	В
J080956.02+502000.9	-34/9/2362	-437/17/12375	970/17/4872	0,1,2	147/43/4016	A
J081855.77+095848.0	3902/13/14787	1821/11/5206	197/0/5631	0,1,2	1954/25/6860	A
J090033.50+421547.0	-347/11/3319	8/26/11593	-988/1/1600	0,1	-360/36/4888	В
J094202.04+042244.5	1181/16/4595	274/7/1761	1686/17/13385	0,1,2	372/40/3356	A
J115954.33+201921.1	1758/7/27583	1385/12/6504	-251/0/1410	0,1,2	1447/19/7525	A
J173352.23+540030.4	1463/5/4095	3385/9/12457	-128/2/2165	0,1,2	254/16/5273	A
J213023.61+122252.0	4591/10/29638	483/17/5852	-23/8/1647	0,1,2	16/35/2474	A
J224956.08+000218.0	1264/22/4067	57/18/2070	467/24/14643	0,1,2	226/65/3160	Α
J230301.45-093930.7	1424/4/4175	-443/0/4973	3675/15/13763	0,1,2	1685/19/9453	A

Note. Column (1): name of the quasars. The names in bold refer to the quasars, the [O III] doublets of which were fitted with two pairs of Gaussians. Column (2): C IV emission-line velocity shift ΔV^{peak} with respect to [O III] λ 5007, REW, and FWHM of the first Gaussian for the C IV line fitting. Column (3): ΔV^{peak} , REW, and FWHM of the second Gaussian for the C IV line fitting. Column (4): ΔV^{peak} , REW, and FWHM of the third Gaussian for the C IV line fitting. Column (5): indexes of Gaussians for the C IV BC. Column (6): ΔV^{peak} , REW, and FWHM of the C IV BC. Column (7): fitting model of the C IV emission line. In Model A, three Gaussians are fitted to the C IV BC and the contribution of the C IV NC is not considered, while in Model B, 2/1 Gaussians are fitted to the C IV BC/NC.

was generally constrained with $\Delta \log(\lambda_{rf} \ (\mathring{A}))$) less than 0.015 and the FWHM less than 35,250 km s⁻¹. The line center and the FWHM of the Mg II NC were tied to that of the H β NC.

The pseudo-continuum-subtracted spectra at 1500 Å < λ < 1700 Å are also modeled with multiple Gaussians. Since the existence of a strong NC in the C IV line is still controversial, which may be difficult to disentangle in the spectra, first we use Model A to fit the region around the C IV line: three Gaussians for the BC of C IV, one for the BC of the He II λ 1640 line, and one for the BC of the O III] λ 1663 line. Each Gaussian fitted to the C IV/He II/O III] BC is constrained with $\Delta \log(\lambda_{\rm rf}$ (Å))) less than 0.015/0.008/0.008 and the FWHM less than $35,250/14,100/14,100\,{\rm km\,s^{-1}}$. Any Gaussian component contributing less than 5% of the total flux is rejected when estimating the FWHMs of the BC of the C IV line.

We then use Model B to fit the C IV line complex: 2/1 Gaussians for the BC/NC of C IV, 1/1 for the BC/NC of the He II line, and 1/1 for the BC/NC of the O III] line. The FWHM and the line center of the NC of these three lines are tied together. Here, the upper FWHM limit of the C IV NC is relaxed to $1600 \, \text{km s}^{-1}$.

Based on a joint analysis of the reduced χ^2 of line fitting from the two models and visual inspection, we identify seven quasars (J015741.57–010629.6, J025021.76–075749.9, J025905.63 +001121.9, J030449.85–000813.4, J075303.34+423130.8, J080819.69+373047.3, and J090033.50+421547.0) with an NC for their C IV lines and adopt the fitting results from Model B. For the other targets, we use Model A to fit the C IV line. The comparisons are presented in the Appendix.

The spectral fitting results for the wavelength range of 1500–1700 Å are shown in Figure 1. Table 2 lists the line shift

 (ΔV) , REW, and FWHM of the three Gaussians for the C IV line of all 19 quasars. Note that each Gaussian fit to the C IV line may not have a robust physical interpretation.

In Table 2, ΔV_i is the line shift of the *i*th Gaussian profile, which is calculated by comparing the fitted line center (λ_i) with the expected rest-frame wavelength of C IV $\lambda 1549$ according to [O III] $\lambda 5007$ (λ_{lab}),

$$\Delta V = \frac{\lambda_{\text{lab}} - \lambda_{\text{i}}}{\lambda_{\text{lab}}} \times c \tag{1}$$

$$\lambda_{\text{lab}} = 1549.06 \times \frac{\lambda_0(\text{[O III]} \lambda 5007)}{5008.24},$$
 (2)

where $\lambda_0([O\,\text{III}]\ \lambda5007)$ is the peak wavelength of the first Gaussian fitting to the $[O\,\text{III}]\ \lambda5007$ and c is the speed of light in a vacuum. 1549.06 and 5008.24 Å are the average rest-frame wavelengths of the unsaturated C IV $\lambda\lambda1548.2$, 1550.8 doublets and the rest-frame wavelength of the $[O\,\text{III}]\ \lambda5007$ line, respectively (Vanden Berk et al. 2001). In each panel of Figure 1, the vertical red dashed line refers to λ_{lab} .

Observations show that even under the simple emission situation in a planetary nebula, the C IV doublet is close to being saturated with an intensity ratio of ~0.8–2.0 (e.g., Feibelman 1983). In that case, assuming equal contribution from both components of the C IV doublet, the average restframe wavelength of C IV is 1549.48 Å. However, to maintain the consistency with a number of previous works (e.g., Vanden Berk et al. 2001; Shen et al. 2011; Shen & Liu 2012), the average rest-frame wavelength of the C IV doublet is adopted as 1549.06 Å under the assumption of the unsaturated C IV doublets with the intensity ratio as 2, though it would generally overestimate the C IV blueshift by ~80 km s⁻¹.

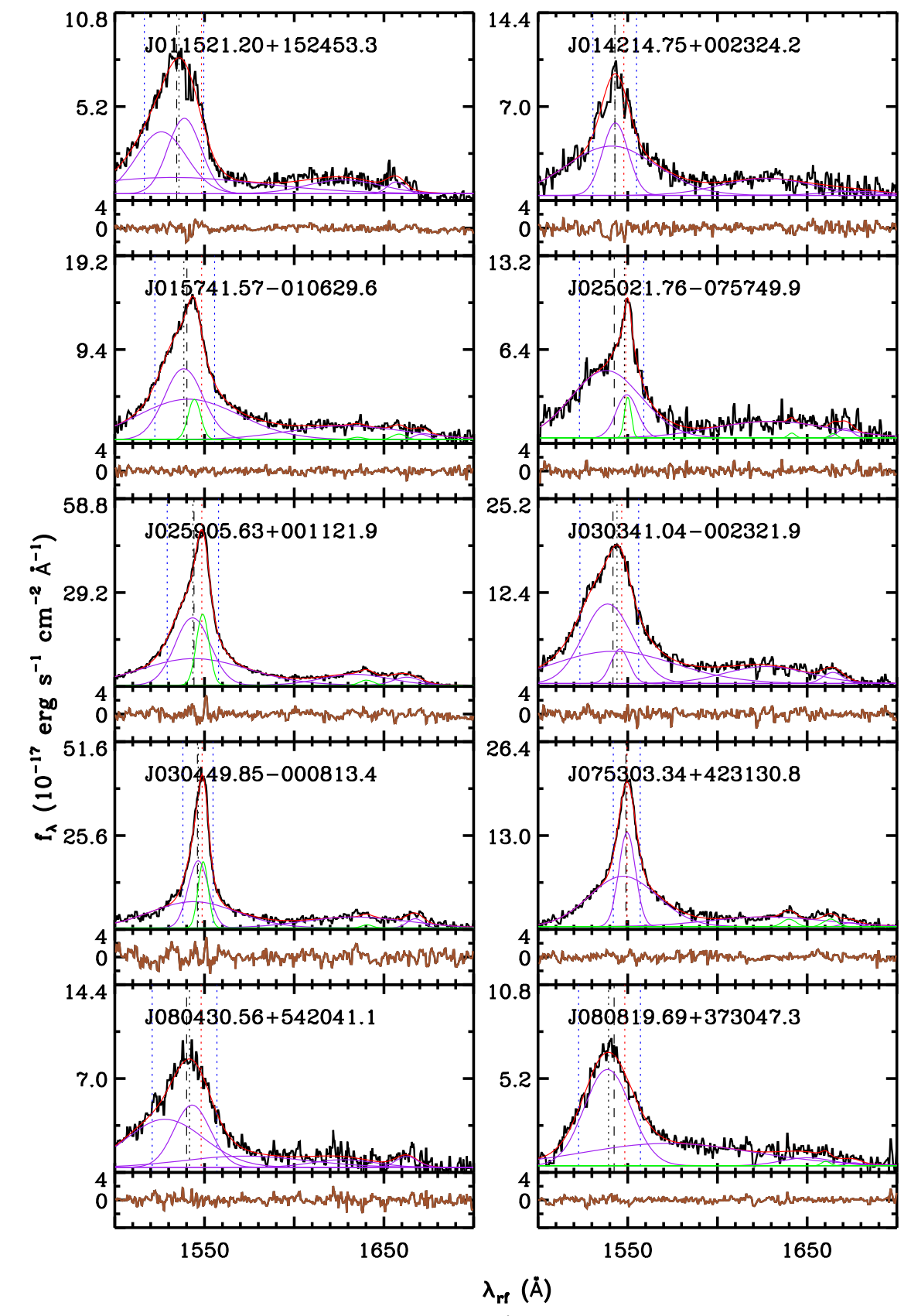


Figure 1. Fitting results of the C IV line complex in the wavelength range of 1500–1700 Å for the 19 quasars, where the spectrum in each panel is shown in black, the combined model fitting is shown in red, the individual Gaussian for the BC is shown in purple, the individual Gaussian for the NC is shown in green, and the fitting residuals are shown in brown. The vertical blue dashed lines from left to right refer to the wavelengths of λ_{blue} and λ_{red} . The vertical red dashed line refers to the wavelength of λ_{lab} . The vertical black dashed and long-dashed lines refer to the wavelengths of λ_0 and λ_{half} , respectively. Except seven quasars (J015741.57 –010629.6, J025021.76–075749.9, J025905.63+001121.9, J030449.85–000813.4, J075303.34+423130.8, J080819.69+373047.3, and J090033.50+421547.0), the C IV line of the other quasars is not fit with an NC.

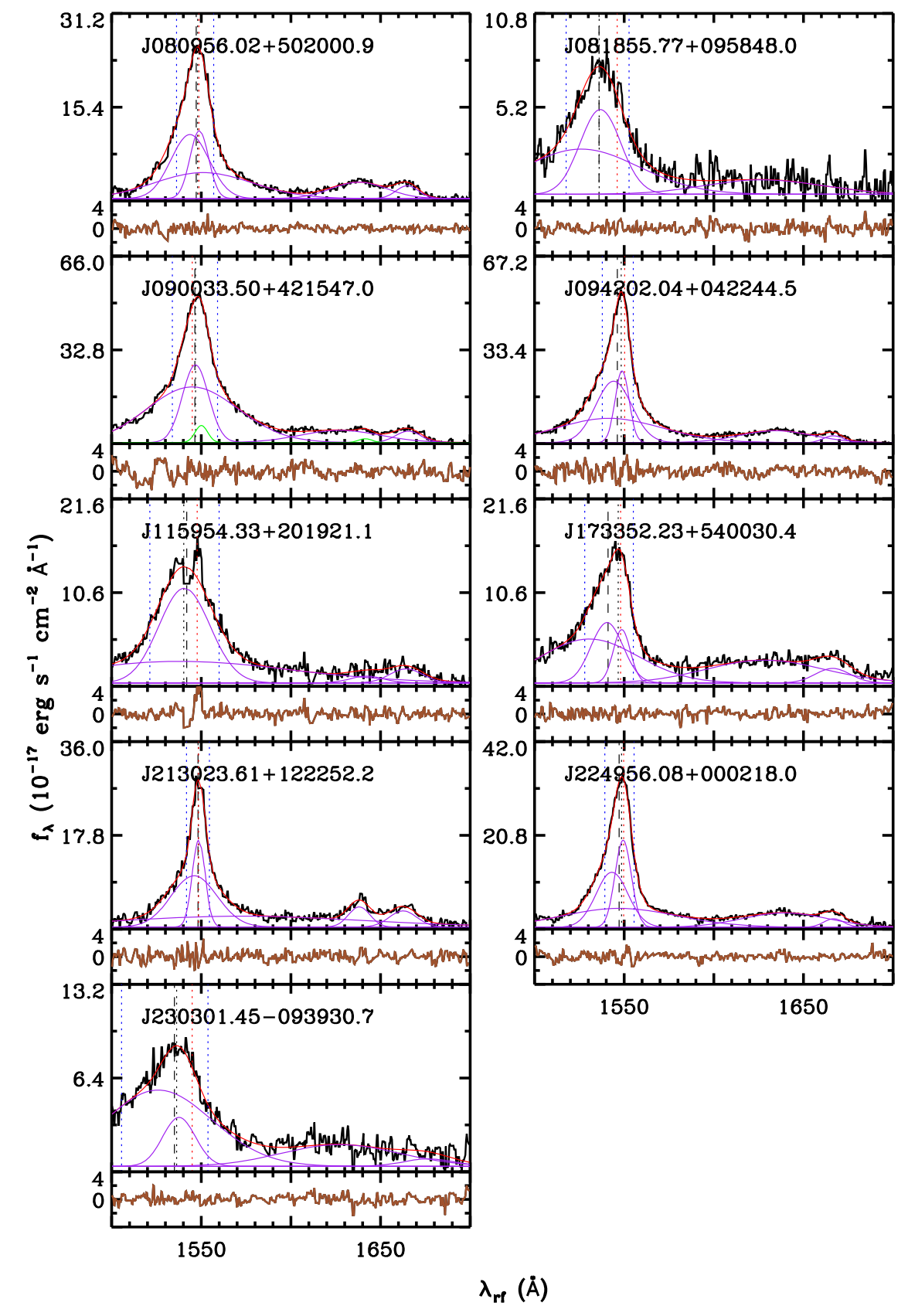


Figure 1. (Continued.)

The line shift $\Delta V_{C\ IV}$ of the C IV BC is calculated with two methods. In the first method, $\Delta V_{C\ IV}^{\rm peak}$ is calculated with the peak wavelength of the best-fitting BC (λ_0) , as shown with the vertical black dashed line in each panel of Figure 1. In the second method, $\Delta V_{C\ IV}^{\rm half}$ is calculated with the wavelength that bisects the commulative total flux of the best-fitting BC $(\lambda_{\rm half})$ as

$$\Delta V_{\text{C IV}}^{\text{half}} = \frac{\lambda_{\text{lab}} - \lambda_{\text{half}}}{\lambda_{\text{lab}}} \times c. \tag{3}$$

The vertical black long-dashed line in each panel of Figure 1 refers to $\lambda_{\rm half}$.

The line shifts calculated with both methods are listed in Table 2. Compared with $\Delta V_{\rm C\,IV}^{\rm peak}$, $\Delta V_{\rm C\,IV}^{\rm half}$ yields a more straightforward way to measure the C IV line shift and is generally subjected to a smaller uncertainty. In our following analysis, the calculated $\Delta V_{\rm C\,IV}^{\rm half}$ values are adopted as the C IV line shifts that are abbreviated as $\Delta V_{\rm C\,IV}$ for simplicity.

We also measure the C IV emission-line asymmetry ($AS_{C IV}$) as the ratio of the widths red and blue of the line centroid from the model fitting of the C IV BC:

$$AS = \ln \frac{\lambda_{\text{red}}}{\lambda_0} / \ln \frac{\lambda_{\text{blue}}}{\lambda_0}, \tag{4}$$

where $\lambda_{\rm red}$ and $\lambda_{\rm blue}$ are the wavelengths at half peak flux red and blue of the line centroid (Shen & Liu 2012), as shown with the vertical blue dashed lines from right to left in each panel of Figure 1.

2.3. Uncertainty Estimation

We apply the Monte Carlo approach to estimate the uncertainties of the fitting parameters (Shen et al. 2011; Shen & Liu 2012). For each object, 100 random mock spectra are created by introducing random Gaussian noises to the original spectrum using the flux density errors of the original spectrum. We then fit the mock spectra with the same fitting strategy. The 1σ dispersion centered on the median of these measurements is taken as the uncertainty, which accounts for the statistical uncertainties and the systematic uncertainties due to the flux errors and the ambiguities in multicomponent spectral fitting, respectively.

Based on the quasars with multiepoch observations obtained from the SDSS-RM project, Sun et al. (2018) justified the uncertainty estimates by exploring the distributions of quasar properties between close-epoch (i.e., rest-frame time interval <2 days) pairs. Taking these as the true uncertainties, the uncertainties estimated using the same Monte Carlo approach are smaller by a factor of $\sim 1.2-1.7$. Therefore, the uncertainties obtained from the Monte Carlo approach should be scaled up by a factor of $\sim 1.2-1.7$.

To estimate the errors caused by the positioning of the continuum, after globally fitting the pseudo-continuum underlying H β and Mg II of the 19 objects, we calculate the difference between the obtained parameters and the corresponding parameters obtained with the method in Section 2.2. Given the median absolute difference of L_{3000} and L_{5100} as ~ 0.012 and 0.043 dex, respectively, the larger one (0.043 dex) can be taken as a rough estimate of the error of the continuum luminosity caused by the positioning of the continuum. In the same way, the error of the line FWHM caused by the positioning of the continuum is $\sim 410 \, \mathrm{km \, s^{-1}}$. These estimated

errors can be propagated into the statistical uncertainties to account for the true errors of the continuum luminosities and the line FWHMs.

3. Results

3.1. Comparison with the H\beta-based BH Mass Estimates

The continuum luminosities and the C IV line properties of the 19 targets are tabulated in Table 3. We use the Spearman's rank correlation coefficient (r) to describe the monotonic correlation between the continuum luminosity at 1350 Å (L_{1350}) and the continuum luminosity at 5100 Å (L_{5100}) . As shown in the left panel of Figure 2, we find a strong correlation between L_{1350} and L_{5100} with $r \sim 0.64$ at a confidence level over 99%. The slope from the bisector linear regression fitting using the BCES estimator (Akritas & Bershady 1996) is 1.1 ± 0.4 , consistent with that in Shen & Liu (2012). As shown in the right panel of Figure 2, there is a poor correlation between the C IV FWHM and the H β FWHM with $r \sim 0.28$ ($p \sim 0.25$), suggesting that the clouds emitting the two features do not fully share the same velocity distribution.

The virial BH mass estimates are expressed as follows:

$$\log\left(\frac{M_{\rm BH,vir}}{M_{\odot}}\right) = a + b \log\left(\frac{L}{10^{44} \text{ erg s}^{-1}}\right) + c \log\left(\frac{\text{FWHM}}{\text{km s}^{-1}}\right),\tag{5}$$

where L and FWHM are the continuum (line) luminosity and the width of one emission line, respectively.

As mentioned in Zuo et al. (2015), the H β -based BH masses are calculated using the calibrations from Vestergaard & Peterson (2006), with (a, b, c) = (0.91, 0.50, 2.00). The Mg II-based BH masses are also considered here for comparison, with (a, b, c) = (1.07, 0.48, 2.00) (Zuo et al. 2015).

The C IV-based BH masses are estimated using the calibration from Vestergaard & Peterson (2006), with (a, b, c) = (0.66, 0.53, 2.00). The errors of the C IV-based BH masses listed in Table 3 are estimated as the 1σ dispersion centered on the median of the measurements from the Monte Carlo approach, not including the intrinsic error of the BH mass SE virial relation (\sim 0.4 dex; Vestergaard 2002; Onken et al. 2004; Vestergaard & Peterson 2006).

Taking the H β -based BH mass estimates as the reference values, we compare the C IV-based and the Mg II-based BH masses with the reference values in Zuo et al. (2015). The histograms of the logarithm of the C IV- and Mg II-based BH mass ratios, i.e., $\log M_{\rm BH}({\rm C\ IV})/M_{\rm BH}({\rm H}\beta)$ and $\log M_{\rm BH}({\rm Mg\ II})/M_{\rm BH}({\rm H}\beta)$, are shown in Figure 3. The values of $\log M_{\rm BH}({\rm C\ IV})/M_{\rm BH}({\rm H}\beta)$ are between -0.85 and 0.67 dex, with a median value of 0.110 ± 0.647 dex. The median value of $\log M_{\rm BH}({\rm Mg\ II})/M_{\rm BH}({\rm H}\beta)$ is 0.041 ± 0.394 dex. Here the scatters are calculated as the inner 50th percentile of the distributions of the logarithm of the mass ratios.

Considering the intrinsic error of the SE virial BH mass estimates as \sim 0.4 dex, all the quasars show consistent Mg II-based BH mass estimates with the corresponding H β -based BH masses, while 63% of quasars show consistent C IV-based BH mass estimates with the H β -based $M_{\rm BH}$ values. The BH mass differences of the other 37% of quasars suggest that the C IV-based BH mass estimates still need to be corrected to better match the H β -based BH masses.

As shown in Table 1, for each quasar in our sample the median S/N per pixel of the SDSS spectra is larger than 15.

 Table 3

 Continuum and Emission-Line Parameters

Name (SDSS)	z	$\log L_{1350}$ (erg s ⁻¹)	FWHM _{C IV} (km s ⁻¹)	$\log M_{\rm BH}^{\rm C\ IV}({\rm VP06}) \atop (M_{\odot})$	REW _{C IV} (Å)	$\Delta V_{ ext{C IV}}^{ ext{peak}} \mid \Delta V_{ ext{C IV}}^{ ext{half}} $ $(ext{km s}^{-1} \mid ext{km s}^{-1})$	Loudness R flag	DR7 T DR7+T NIR T
(1)	(2)	(3)	(4)	(5)	(6)	(7)	(8)	(9)
J011521.20+152453.3	3.443	$46.95 \pm < 0.01$	6483 ± 200	9.85 ± 0.03	27 ± 1	$2433 \pm 352/2678 \pm 277$	-1/-1	071205/071205/111022
J014214.75+002324.2	3.379	$47.01 \pm < 0.01$	4730 ± 227	9.61 ± 0.04	24 ± 1	$962 \pm 105/965 \pm 100$	0/-1	000901/000901/111021
J015741.57-010629.6	3.572	$46.99 \pm < 0.01$	6489 ± 149	9.87 ± 0.02	45 ± 1	$1918 \pm 75/1590 \pm 61$	0/-1	001123/100910/111021
J025021.76-075749.9	3.337	$47.03 \pm < 0.01$	6983 ± 992	9.95 ± 0.12	18 ± 1	$140 \pm 776/1233 \pm 233$	0/-1	001223/001223/111021
J025905.63+001121.9	3.373	$47.16 \pm < 0.01$	5562 ± 116	9.83 ± 0.02	55 ± 1	$957 \pm 54/847 \pm 37$	1/5.5	001223/101007/111021
J030341.04-002321.9	3.233	$47.16 \pm < 0.01$	6383 ± 386	9.95 ± 0.05	34 ± 1	$511 \pm 261/946 \pm 217$	0/-1	000930/011023/111022
J030449.85-000813.4	3.287	$47.38 \pm < 0.01$	3261 ± 892	9.48 ± 0.19	21 ± 1	$421 \pm 137/506 \pm 106$	0/-1	000930/000930/111020
J075303.34+423130.8	3.590	$47.22 \pm < 0.01$	2903 ± 731	9.29 ± 0.15	27 ± 1	$22 \pm 93/117 \pm 42$	1/2645.3	000930/091213/111020
J080430.56+542041.1	3.759	$47.10 \pm < 0.01$	7041 ± 253	10.00 ± 0.031	30 ± 1	$1258 \pm 155/1570 \pm 102$	0/-1	050114/050114/111022
J080819.69+373047.3	3.480	$46.85 \pm < 0.01$	6714 ± 341	9.82 ± 0.04	31 ± 1	$1755 \pm 120/1150 \pm 149$	0/-1	011210/100312/111021
J080956.02+502000.9	3.281	$47.03 \pm < 0.01$	4016 ± 73	9.48 ± 0.02	43 ± 1	$147 \pm 176/296 \pm 163$	0/-1	040326/101117/111022
J081855.77+095848.0	3.700	$47.09 \pm < 0.01$	6860 ± 479	9.97 ± 0.06	25 ± 1	$1954 \pm 282/1967 \pm 168$	0/-1	070218/070218/111021/22
J090033.50+421547.0	3.290	$47.49 \pm < 0.01$	4888 ± 522	9.89 ± 0.08	36 ± 1	$-360 \pm 205/-282 \pm 196$	1/2.1	020120/120226/120415
J094202.04+042244.5	3.276	$47.37 \pm < 0.01$	3356 ± 51	9.50 ± 0.01	$40 \pm < 1$	$372 \pm 111/788 \pm 110$	0/-1	011223/010411/120415
J115954.33+201921.1	3.426	$47.40 \pm < 0.01$	7525 ± 310	10.21 ± 0.041	$19 \pm < 1$	$1447 \pm 533/1126 \pm 56$	0/-1	080109/080109/120416
J173352.23+540030.4	3.432	$47.45 \pm < 0.01$	5273 ± 136	9.93 ± 0.02	16 ± 1	$254 \pm 712/1355 \pm 703$	1/14.0	000929/010331/120415
J213023.61+122252.0	3.272	$47.10 \pm < 0.01$	2474 ± 77	9.09 ± 0.03	35 ± 1	$16 \pm 31/46 \pm 36$	-1/-1	020705/020705/111021
J224956.08+000218.0	3.311	$46.90 \pm < 0.01$	3160 ± 42	9.20 ± 0.01	65 ± 1	$226 \pm 35/490 \pm 25$	0/-1	021112/101002/111022
J230301.45-093930.7	3.492	$47.27 \pm < 0.01$	9453 ± 453	10.34 ± 0.041	19 ± 1	$1685 \pm 540/1923 \pm 392$	0/-1	011215/011215/111020

Note. Column (1): name of the quasars. Column (2): redshift measured from the H β and the [O III] doublets of the NIR spectra. Column (3): continuum luminosity at 1350 Å. Column (4): FWHM of the C IV BC. Column (5): C IV line-based BH masses estimated using the calibration from Vestergaard & Peterson (2006). The uncertainties quoted are only from statistical errors and not including the intrinsic uncertainties of the SE virial BH mass estimates as \sim 0.4 dex (Vestergaard 2002). Column (6): REW of the C IV emission line. Column (7): C IV emission-line velocity shifts $\Delta V_{\text{C IV}}^{\text{peak}}$ and $\Delta V_{\text{C IV}}^{\text{half}}$ with respect to [O III] λ 5007. Column (8): FIRST radio flag: -1 = not in FIRST footprint; 0 = FIRST undetected; 1 = core dominant. Radio-loudness $R = f_{\text{6cm}}/f_{2500}$. Column (9): date when the SDSS DR7/SDSS DR7+/NIR spectroscopy were taken, e.g., 071110 referring to 2007 November 10.

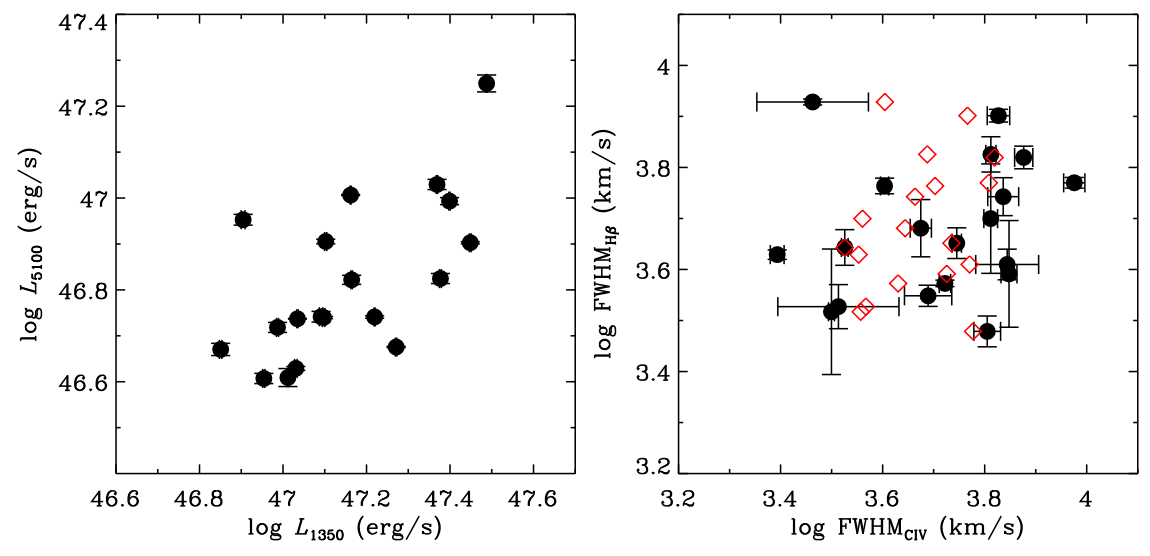


Figure 2. Left panel: correlation between log L_{1350} and log L_{5100} . Right panel: correlation between log FWHM_{H β} and log FWHM_{C IV}, where the red diamonds refer to the corrected log FWHM_{C IV} using Equation (6). More details can be found in Section 3.4.

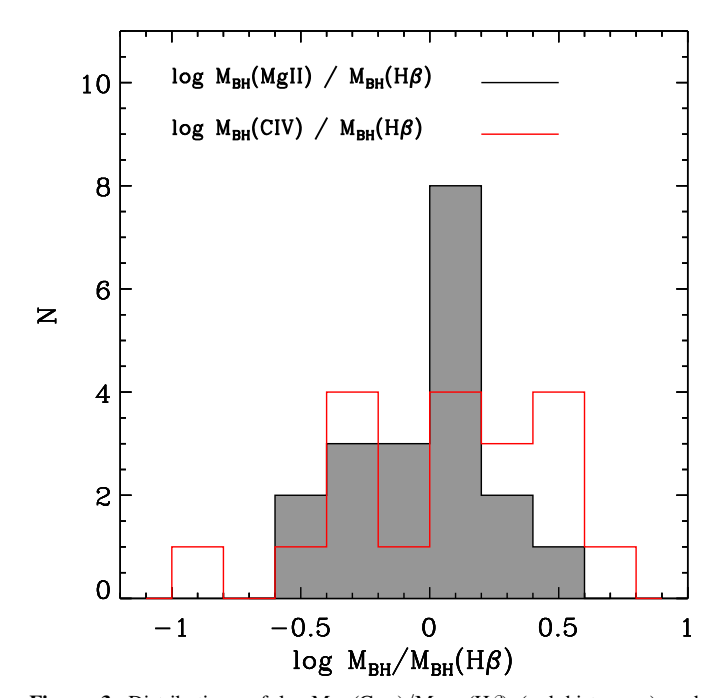


Figure 3. Distributions of log $M_{BH}(C \text{ IV})/M_{BH}$ (H β) (red histogram) and log $M_{BH}(Mg \text{ II})/M_{BH}(H\beta)$ (gray shaded histogram).

For the NIR spectrum of each quasar, the median S/N per spectral resolution element of 3 pixels is no less than 10. Using the SDSS DR7 sample, Shen et al. (2011) found that the bias affecting the continuum luminosities and FWHMs during the spectral measurements are negligible even if S/N is reduced to as low as \sim 5. This is further confirmed in Runnoe et al. (2013). Given the relatively high S/N of the NIR and optical spectra in our sample, we argue that the difference of the S/N of SDSS optical spectra and NIR spectra of our quasars makes a small contribution to the differences between the C IV- and H β -based BH masses.

The continuum variation is typically at the level of \sim 0.1 mag for average SDSS quasars (MacLeod et al. 2012; Zuo et al. 2012). Since the luminosity enters into the BH mass estimates as the square root, the luminosity uncertainty does not make a

large contribution to the BH mass estimates (Coatman et al. 2017). For the line shape variability, Wilhite et al. (2007) found that the variation of the C IV line FWHM is less than 0.05 dex, using 615 high-z quasars with spectra observed at two epochs. They concluded that the inherent continuum and line shape variability contributes \sim 20% to the BH mass variations (\sim 0.08 dex) between different epochs.

As listed in Table 1, the time differences between the NIR spectroscopy and the SDSS spectroscopy range from 49 days to 12 yr, corresponding to 11 days–2.6 yr in the rest frame of quasars ($\Delta T_{\rm rf}$), where 8 out of the 19 quasars were observed with time differences larger than 2 yr in the rest frame of quasars. The absolute logarithm of the median BH mass ratio (log $M_{\rm BH}({\rm C~IV})/M_{\rm BH}({\rm H}\beta)$) for quasars with $\Delta T_{\rm rf} < 2$ yr is measured to be 0.11 \pm 0.46 dex, while for quasars with $\Delta T_{\rm rf} > 2$ yr, the absolute logarithm of the median BH mass ratio is 0.43 \pm 0.53 dex.

However, we find that the median $\log M_{\rm BH}({\rm H}\beta)$ value for quasars with $\Delta T_{\rm rf} < 2$ yr is larger by 0.23 dex than that for quasars with $\Delta T_{\rm rf} > 2$ yr, and the median $\log M_{\rm BH}({\rm C~IV})$ value for quasars with $\Delta T_{\rm rf} < 2$ yr is smaller by 0.08 dex than that for quasars with $\Delta T_{\rm rf} < 2$ yr. That means that the relatively larger $|\log M_{\rm BH}({\rm C~IV})/M_{\rm BH}({\rm H}\beta)|$ with $\Delta T_{\rm rf} > 2$ yr is mainly due to the distributions of the C IV- and H β -based BH masses with the observing time difference, which are not related to the quasar intrinsic properties.

3.2. Dependences of the Mass Differences on Different Parameters

To investigate whether the logarithm of the mass ratios depends on the C IV emission-line properties, in Equation (5) we assume that there is no dependence on the FWHM by fixing c as 0 and then calibrate the C IV-based BH masses to the reference H β -based BH masses using the LINMIX_ERR approach (Kelly 2007). If b is adopted as 0.530 (Vestergaard & Peterson 2006), the best-fitting result yields the a value as 8.01 ± 0.26 . The median logarithm of the mass ratio is 0.025 ± 0.360 .

To investigate the dependence of the mass ratios on the continuum luminosities, in Equation (5) we assume that there is

Table 4 log $M_{\rm BH}$ from the C IV Emission Line Using Different Calibrations versus the Reference H β -based log $M_{\rm BH}$ Estimates Using the Calibration in Vestergaard & Peterson (2006)

<i>a</i> (1)	<i>bc</i> (2)	c (3)	$\Delta \log M_{ m BH}$ (4)	σ (5)
0.66	0.53	2.0	0.110	0.647
8.01 ± 0.26	0.53	0	0.025	0.360
2.26 ± 0.38	0	2.0	0.006	0.432

no dependence on L by fixing b as 0 and then calibrate the C IV-based BH masses to the reference BH masses using the LINMIX_ERR approach (Kelly 2007). If c is adopted as 2.00 (Vestergaard & Peterson 2006), the best-fitting a value is 2.26 ± 0.38 . The median logarithm of the mass ratio is 0.006 ± 0.432 .

The median logarithm of the mass ratios and fitting results are tabulated in Table 4. We find that under the aforementioned assumptions, the scatters are large. Moreover, the scatter is smaller when the dependence of the BH mass estimates on the FWHM is assumed to be zero. It indicates that the scatter of the mass differences is more related to the line properties than the continuum luminosities.

For the 19 targets, we further investigate the Spearman rank correlations between the logarithm of the mass ratios $\log M_{\rm BH}({\rm C~IV})/M_{\rm BH}({\rm H}\beta)$ and detailed spectral properties, as tabulated in Table 5. There is a strong correlation with FWHM_{C IV}/FWHM_{H β} ($r\sim0.98,~p<0.01$), FWHM_{C IV} ($r\sim0.67,~p<0.01$), a moderate correlation with the C IV blueshift $\Delta V_{\rm C~IV}$ ($r\sim0.54,~p\sim0.02$), and a moderate anticorrelation with the C IV asymmetry ${\rm AS_{C~IV}}$ ($r\sim-0.62,~p<0.01$). However, we note that the strong relation with FWHM_{C IV}/FWHM_{H β} is simply due to the fact that the calculated $M_{\rm BH}({\rm C~IV})/M_{\rm BH}({\rm H}\beta)$ values are proportional to (FWHM_{C IV}/FWHM_{H β}). No significant correlations with other parameters are found, such as the luminosity or the logarithm of the luminosity ratio.

It suggests that the logarithm of the mass ratio is mainly affected by the line properties, such as FWHM_{C IV}, $\Delta V_{C IV}$, and AS_{C IV}. The dependence of $\log M_{\rm BH}({\rm C IV})/M_{\rm BH}({\rm H}\beta)$ on the observed parameters is shown in Figure 4, including the dependences on FWHM_{C IV}, $\Delta V_{\rm C IV}$, and AS_{C IV}. Influences caused by line properties, such as the blueshift and asymmetry could be taken into account to further reduce the difference between the C IV- and H β - based BH mass estimates.

3.3. Correlation between the C IV FWHM and the C IV Blueshift

The distribution of the derived C IV blueshifts is shown in Figure 5. Among the 19 quasars, 18 quasars exhibit positive C IV blueshifts, with the median value as $1126\,\mathrm{km\,s}^{-1}$ and the inner 50th percentile of the distribution as $1064\,\mathrm{km\,s}^{-1}$. A total of 14/19 of the quasars show C IV blueshifts larger than $500\,\mathrm{km\,s}^{-1}$. Uncertainties of the C IV blueshifts range from 25 to $703\,\mathrm{km\,s}^{-1}$, with the median value at $110\,\mathrm{km\,s}^{-1}$. The uncertainties are generally larger for larger blueshifts.

As shown in Figure 6, for our sample with $L_{\rm bol} \sim 10^{47.5} - 10^{48.3} \, {\rm erg \, s^{-1}}$, the C IV FWHM strongly correlates with the C IV blueshift, with the Spearman correlation coefficient as 0.78 (p < 0.01). Consistent results were found in many previous studies (e.g., Richards et al. 2002; Sulentic et al. 2007;

Variable	r	p
(1)	(2)	(3)
${\log L_{1350}}$	0.31	0.19
$\log L_{5100}$	0.04	0.86
$\log L_{1350}/L_{5100}$	0.20	0.42
FWHM _{C IV}	0.67	< 0.01
$FWHM_{H\beta}$	-0.40	0.09
$FWHM_{C \text{ IV}}/FWHM_{H\beta}$	0.98	< 0.01
C IV blueshift $\Delta V_{\rm C~IV}$	0.54	0.02
C IV asymmetry $AS_{C\ IV}$	-0.62	< 0.01

Note. Column (2): Spearman rank correlation coefficient r. Column (3): significance of r deviated from the null hypothesis.

Shen & Liu 2012; Coatman et al. 2016; Sun et al. 2018; Vietri et al. 2018; Marziani et al. 2019), suggesting that the C IV FWHM is likely a combination of a virialized component and an outflow component.

For the large DR7 quasar sample, the C IV blueshifts relative to the Mg II line can be estimated from the cataloged velocity shifts of C IV and the velocity shifts of broad Mg II relative to the systematic redshifts (Schneider et al. 2010; Shen et al. 2011). For a better comparison, we superimpose analog data in contours, i.e., the C IV blueshifts relative to the broad Mg II line and the C IV line FWHM, from the large DR7 quasar sample of 44,426 quasars with 1.5 < z < 5.0 located in the Faint Images of the Radio Sky at Twenty cm (FIRST) footprint with radioloudness less than 10, nonzero REW_{C IV}, FWHM_{C IV}, $\log L_{1350}$, and $\log R_{\rm EDD}$ values (Shen et al. 2011). The radio-loudness (R) is defined as the ratio of the flux density at rest-frame 6 cm to the flux density at 2500 Å (Jiang et al. 2007; Shen et al. 2011). The border lines represent the 25th, 50th, 75th, and 95th percentile contours centered at the maximum probability point. Similar to Coatman et al. (2016), we find that the FWHMs of quasars with large C IV blueshifts ($\approx 1500 \, \text{km s}^{-1}$) are about 2 times higher than those with moderate blueshifts $(\approx 300 \, \text{km s}^{-1}).$

3.4. Corrections of the C IV FWHM

Given the correlation between FWHM $_{\rm C\,IV}/{\rm FWHM}_{\rm H\beta}$ and the C IV blueshift ($r\sim056,~p\sim0.01$), FWHM $_{\rm C\,IV}$ can be calibrated with the C IV blueshift to get better agreement with FWHM $_{\rm H\beta}$, which in turn results in a slightly more accurate BH mass estimate.

The following equation is fitted to the data using the LINMIX_ERR procedure:

$$FWHM_{CIV}/FWHM_{H\beta} = \alpha + \beta (\Delta V/1000 \text{ km s}^{-1}), \quad (6)$$

where ΔV is the C IV blueshift. For the 18 quasars with positive ΔV values, the best-fitting results are $\alpha=0.67\pm0.20$ and $\beta=0.41\pm0.17$, which is shown as the black line in the left panel of Figure 7. Then, the corrected FWHM_{C IV} is calculated as FWHM_{C IV} $/(\alpha+\beta)$ ($\Delta V/1000~{\rm km~s}^{-1}$)). The corrected FWHM_{C IV} values based on this calibration are also displayed in the right panel of Figure 2 as the red symbols.

The red dashed line in Figure 7 refers to the best-fitting relation for the 230 high-luminosity, 1.5 < z < 4.0 quasars as shown in Figure 6 of Coatman et al. (2017)

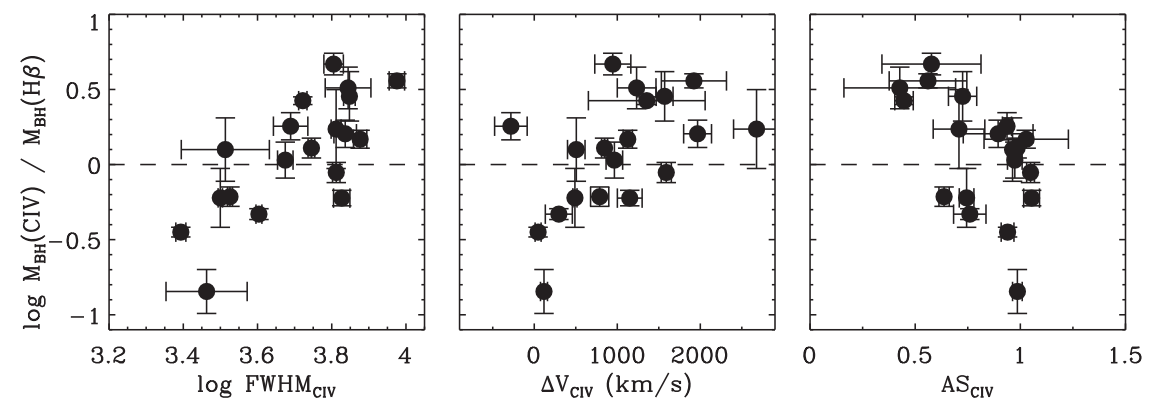


Figure 4. Dependence of the logarithm of the C IV-to-H β BH mass ratios on FWHM_{C IV} (left), the C IV blueshifts (middle), and the C IV asymmetries (right). The dashed line in each panel refers to the situation where the C IV- and H β -based BH masses are equal.

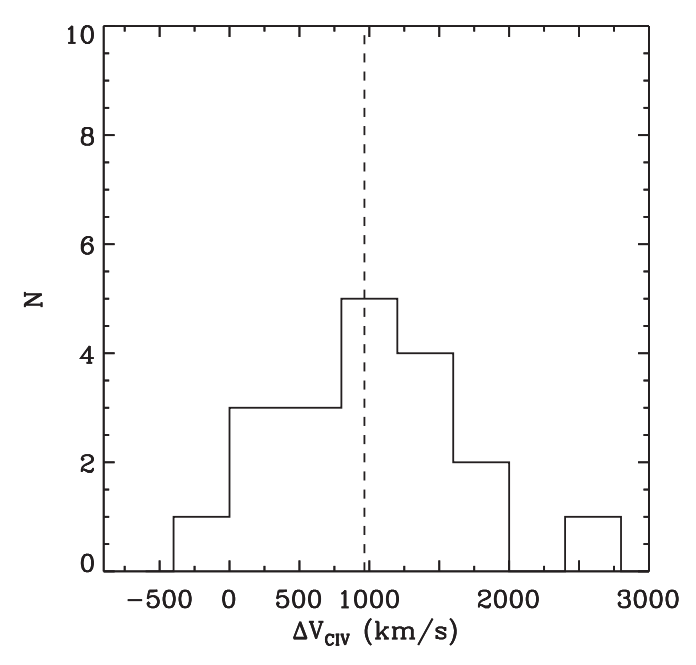


Figure 5. Distribution of the C IV emission-line blueshifts with respect to [O III] $\lambda 5007$.

with $\alpha=0.61\pm0.04$ and $\beta=0.36\pm0.03$. The C IV blueshifts in Coatman et al. (2017) are defined as $c(1549.48-\lambda_{\rm half})/1549.48$, where 1549.48 Å is the rest-frame wavelength of the C IV doublet assuming equal contribution from both components.

Given the anticorrelation between FWHM_{C IV}/FWHM_{H β} and the C IV asymmetry, the C IV FWHM can also be calibrated with the C IV asymmetry to better agree with the H β FWHM using the LINMIX_ERR procedure:

$$FWHM_{CIV}/FWHM_{H\beta} = \alpha + \beta AS_{CIV}.$$
 (7)

For the 19 targets, the best-fitting results are $\alpha = 2.03 \pm 0.52$ and $\beta = -1.1 \pm 0.62$. The fitting result is shown as the black line in the right panel of Figure 7.

3.5. Corrections of the CIV-based Virial BH Mass Estimates

Using the corrected FWHM_{C IV} and the scaling relations in Vestergaard & Peterson (2006) for the C IV line, we calculate the corrected BH masses $M_{C \text{ IV,corr}}$. The left panel of Figure 8 compares the C IV- and H β - based BH masses before and after applying the blueshift-based correction to the C IV FWHM for

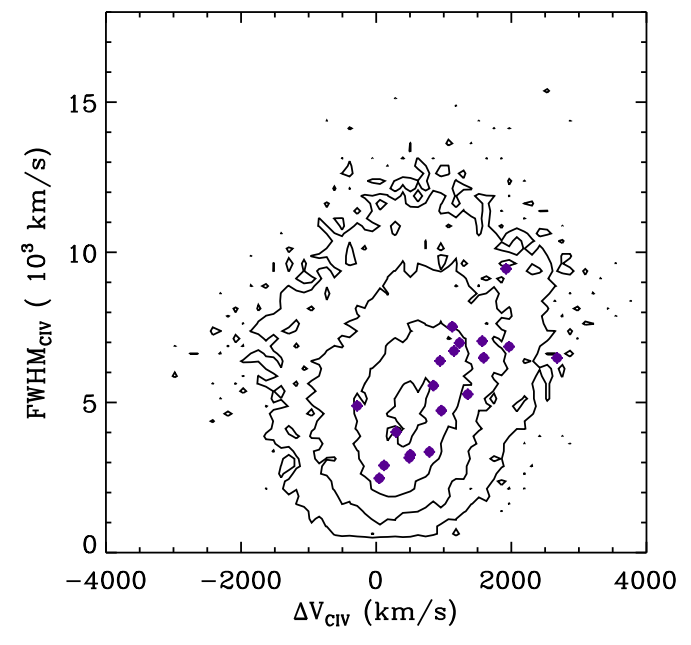


Figure 6. Correlation between FWHM_{C IV} and the C IV blueshifts for the 18 quasars with positive $\Delta V_{\rm C IV}$ values. The contours are the analog data from the large DR7 quasar sample of 44,426 quasars with the C IV FWHW values and the C IV blueshifts relative to the broad Mg II line. The lines refer to the 25th, 50th, 75th, and 95th percentile contours centered at the maximum probability point.

the 18 quasars with positive $\Delta V_{C\,{
m IV}}$. The reduction in scatter between the C IV- and H β -based BH masses can be seen in the reduction in the width of the distribution of the mass differences. Before the correction, the median difference between the masses is 0.110 dex and the scatter is 0.647 dex. After correcting the C IV FWHM for the nonvirial contribution using the $\Delta V_{C\,{
m IV}}$, the median difference is reduced to -0.032 dex with the scatter as 0.424 dex.

The right panel of Figure 8 compares the C IV- and H β -based BH masses before and after applying the C IV asymmetry-based correction to the C IV FWHM for the 19 quasars. After the correction, the median difference is -0.065 dex with the scatter as 0.643 dex. For the target J075303.34 +423130.8 with the largest absolute mass difference, the logarithms of the C IV-to-H β mass ratio before and after the asymmetry-based correction are -0.845 and -0.797 dex, respectively. Excluding this target, the median difference before the asymmetry-based correction is 0.169 ± 0.639 ,

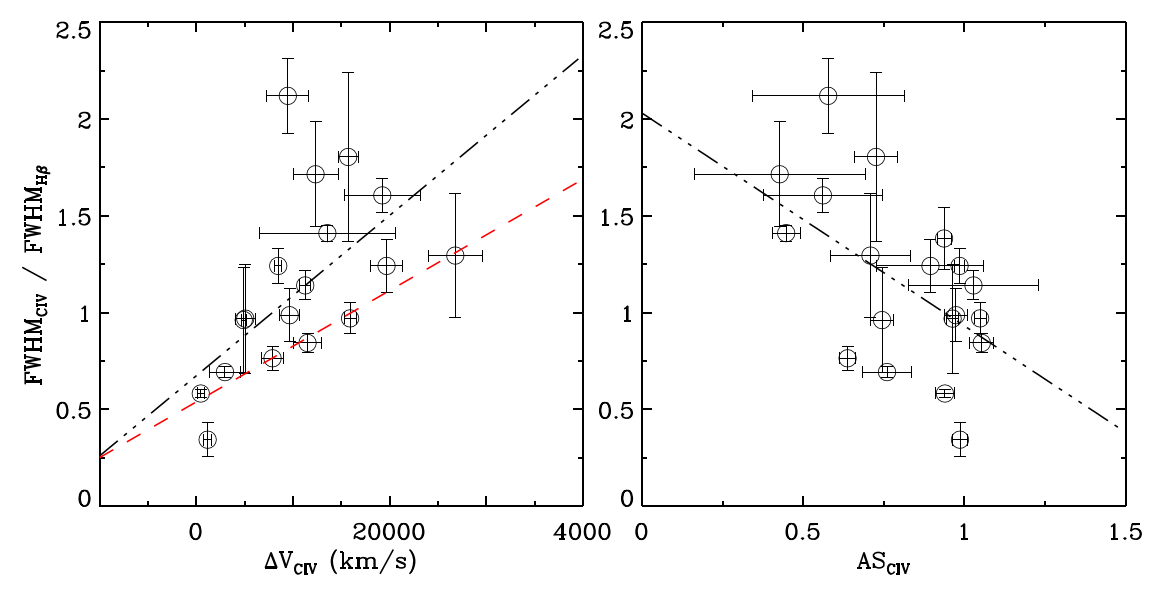


Figure 7. Left: Correlation between FWHM $_{C\ IV}$ /FWHM $_{H\beta}$ and the C IV blueshift for the 18 quasars with positive $\Delta V_{C\ IV}$, where the black dotted–dashed line refers to the best-fitting relation for the 18 quasars and the red dashed line represents the best-fitting relation for the 230 high-luminosity, 1.5 < z < 4.0 quasars shown in Figure 6 of Coatman et al. (2017). Right: Correlation between FWHM $_{C\ IV}$ /FWHM $_{H\beta}$ and the C IV asymmetry for the 19 quasars, where the black dotted–dashed line refers to the best-fitting relation for the 19 quasars.

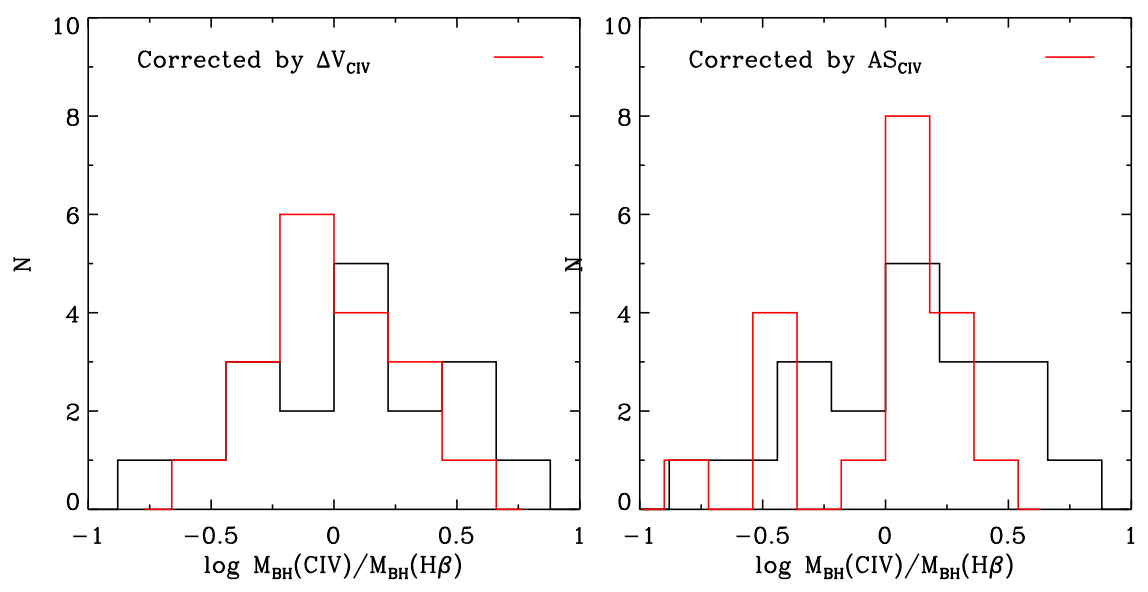


Figure 8. Left: for the 18 quasars with positive blueshifts, comparison of the C IV- and H β -based BH masses before (black histogram) and after applying the C IV blueshift-based correction to the C IV FWHMs (red histogram). Right: for the 19 quasars, comparison of the C IV- and H β -based BH masses before (black histogram) and after applying the C IV asymmetry-based correction to the C IV FWHMs (red histogram).

which reduces to 0.123 ± 0.359 after the correction. Therefore, the correction based on the C IV asymmetry reduces the scatter of $\log M_{\rm BH}({\rm C\,IV})/M_{\rm BH}({\rm H}\beta)$ by less than 0.1 dex and by ${\sim}0.3$ dex if the target with the largest absolute mass difference is excluded.

4. Discussion

4.1. Comparison with Previous Works

Considering the intrinsic error of the SE virial BH mass estimates as \sim 0.4 dex, no significant differences between the C IV-based and the H β -based BH masses are found in some previous studies (Vestergaard 2002; Vestergaard & Peterson 2006; Greene et al. 2010; Assef et al. 2011). For our high-z luminous

quasars, the median logarithm of the C IV-to-H β mass ratios is 0.110 dex, but the scatter is 0.647 dex, with 63% quasars showing mass residuals less than 0.4 dex. It suggests that the C IV-based BH mass estimates still need to be corrected to reduce the difference with the H β -based BH masses (Denney 2012; Trakhtenbrot & Netzer 2012; Park et al. 2013; Runnoe et al. 2013; Coatman et al. 2017; Sulentic et al. 2017; Mejía-Restrepo et al. 2018; Marziani et al. 2019).

Among the 1350 and 5100 Å continuum luminosities, redshift, Eddington ratio, C IV blueshift, C IV asymmetry, and the logarithm of the ratio of the UV and optical continuum luminosities, Assef et al. (2011) found that only the correlation between $logM_{BH}(C\ IV)/M_{BH}(H\beta)$ and the logarithm of the ratio of continuum luminosities is most significant. They

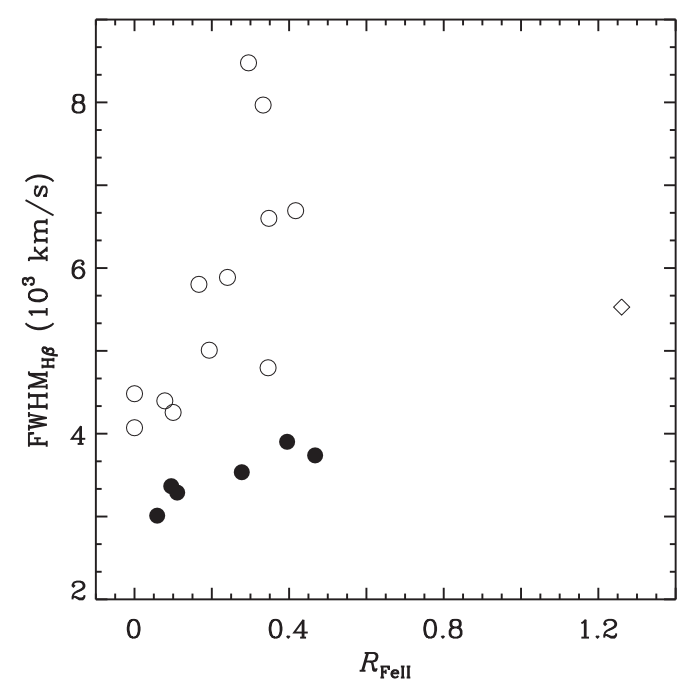


Figure 9. Distribution of the quasars in the optical EV1 plane, FWHM $_{\rm H\beta}$ vs. $R_{\rm Fe~II}$. The Population A1 quasars with FWHM $_{\rm H\beta} < 4000~{\rm km~s}^{-1}$ and $R_{\rm Fe~II} < 0.5$ are denoted as filled circles, the Population B quasars with FWHM $_{\rm H\beta} > 4000~{\rm km~s}^{-1}$ and $R_{\rm Fe~II} < 0.5$ are denoted as open circles, and the remaining quasar is shown as the diamond.

suggested that the dispersions in previous comparisons between the C IV- and the H β -based $M_{\rm BH}$ estimates are mainly due to the continuum luminosities rather than any other properties of the lines.

Shen & Liu (2012) found that the better correlation between the FWHMs of the C IV and H β lines seen in Assef et al. (2011) is essentially driven by the objects with lower luminosity. Marziani et al. (2019) suggested that the 10 gravitationally lensed quasars in Assef et al. (2011) might have a preferential section of Population B quasars with FWHM_{H β} > 4000 km s⁻¹ and better agreement between H β and C IV line widths.

Here, based on an independent high-redshift and high-luminosity quasar sample, we find a strong correlation between $\log M_{\rm BH}({\rm C\,IV})/M_{\rm BH}({\rm H}\beta)$ and the C IV blueshift, the C IV asymmetry, and the C IV FWHM, as tabulated in Table 5. Different from the result in Assef et al. (2011), these correlations are more significant than that with the logarithm of the ratio of the continuum luminosities.

The distribution of quasars in the FWHM_{H β}– $R_{\rm Fe\ II}$ plane is shown in Figure 9. With the classification scheme in Marziani et al. (2010, 2019), there are six Population A1 quasars (FWHM_{H β} < 4000 km s⁻¹, $R_{\rm Fe\ II}$ < 0.5), 12 Population B quasars (FWHM_{H β} > 4000 km s⁻¹, $R_{\rm Fe\ II}$ < 0.5), and the remaining one is J081855.77+095848.0 (FWHM_{H β} > 4000 km s⁻¹, $R_{\rm Fe\ II}$ < 0.5). The correlations between FWHM_{C IV} and FWHM_{H β} of the quasars in both Population A1 and Population B are insignificant, with $r \sim 0.43$ ($p \sim 0.40$) and $r \sim 0.22$ ($p \sim 0.50$), respectively. The correlation between log L_{1350} and log L_{5100} for the Population B quasars is strong with $r \sim 0.76$ ($p \sim 0.004$), while there is no correlation between the continuum luminosities for the Population A1 quasars. Note that the number of Population A1 quasars is only 6, which could bias the correlation analysis. Nevertheless, the poor relations between the FWHMs in both the Population A1 and Population B quasars suggest that the differences between

the line widths exist and may contribute to the differences between the C IV- and H β -based BH masses.

From Figure 4, for the AGNs with C IV blueshift larger than $1000\,\mathrm{km\,s}^{-1}$, the median C IV-based BH mass is roughly overestimated by a factor of $\sim\!2$ compared to the H β -based BH masses. It is roughly consistent with the result found in Coatman et al. (2016) but with a smaller overestimate value. For quasars with C IV blueshift larger than $2000\,\mathrm{km\,s}^{-1}$, the C IV-based BH masses overestimate the H α -based BH masses by a factor of $\sim\!5$ (Coatman et al. 2016).

Further using a large sample of 230 high-luminosity $(L_{\rm bol} \sim 10^{45.5} - 10^{48} \, {\rm erg \ s^{-1}})$ and 1.5 < z < 4 quasars, Coatman et al. (2017) corrected the BH masses based on the blueshift-corrected C IV FWHMs, where the blueshifts are calculated with $\lambda_{\rm half}$. After the correction, the scatter between the corrected C IV-based and the Balmer line-based BH masses decreases from 0.4 to 0.24 dex. Marziani et al. (2019) confirmed the applicability of correcting FWHM_{C IV} using the C IV blueshift and the luminosity for 76 quasars with $L_{\rm bol} \sim 10^{44} - 10^{48.5} \, {\rm erg \ s^{-1}}$ and 0 < z < 3.

On correcting the C IV-based BH mass estimates, previous studies have presented other methods based on the parameters relatively independent of the redshift estimates, such as reducing the dependence of the BH masses on the emission-line width (Shen & Liu 2012; Park et al. 2013, 2017), the continuum-subtracted peak flux ratio of the ultraviolet emission-line blend of Si IV+O IV relative to C IV (Runnoe et al. 2013), and the C IV shape (Denney 2012).

Mejía-Restrepo et al. (2018) suggested that these correction methods based on the line peak ratios or blueshifts are of limited applicability. This is because most of them depend on correlations that are not driven by an interconnection between the line width of C IV and that of the low ionization lines. Coatman et al. (2017) found that the correction based on the C IV blueshifts $\Delta V_{C IV}$ yields no systematic bias to correct the BH masses at different blueshifts. It hints that correcting the C IV-based BH mass estimates using $\Delta V_{\text{C IV}}$ is still valuable. In our work, for the luminous quasars $(L_{bol} > 10^{47.5} \,\mathrm{erg \, s}^{-1})$, before the correction, the median difference is 0.110 dex, but the scatter is as large as 0.647 dex. After the correction using $\Delta V_{\rm C\,IV}$, the median difference is -0.032 dex and the scatter is reduced from 0.647 to 0.424 dex. This large scatter indicates that the correction using $\Delta V_{C IV}$ is still not sufficient, and other intrinsic properties have to be taken into account in the corrections of the C IV-based virial BH mass estimates.

Estimates of $\Delta V_{C\,IV}$ require accurate redshift estimates, which can be obtained with rest-frame optical spectra. However, if a rest-frame optical spectrum is available, it is unnecessary to correct the C IV-based BH masses based on the blueshift. Therefore, a correction using only the information around the C IV line is required, such as the $AS_{C\,IV}$. In our sample, after using the correction with $AS_{C\,IV}$, the median difference is -0.065 dex and the scatter decreases by less than 0.1 dex. If the target with the largest absolute mass difference is excluded, the scatter is reduced by $\sim\!0.3$ dex. Investigations on whether $AS_{C\,IV}$ and other properties can be used for the correction of FWHM $_{C\,IV}$ will benefit significantly from a larger sample.

On the other hand, if the systemic redshift can be estimated with an improved method through only the rest-frame UV spectra, such as the principal-component-analysis-based redshift estimates, the C IV-based BH mass estimates can still be

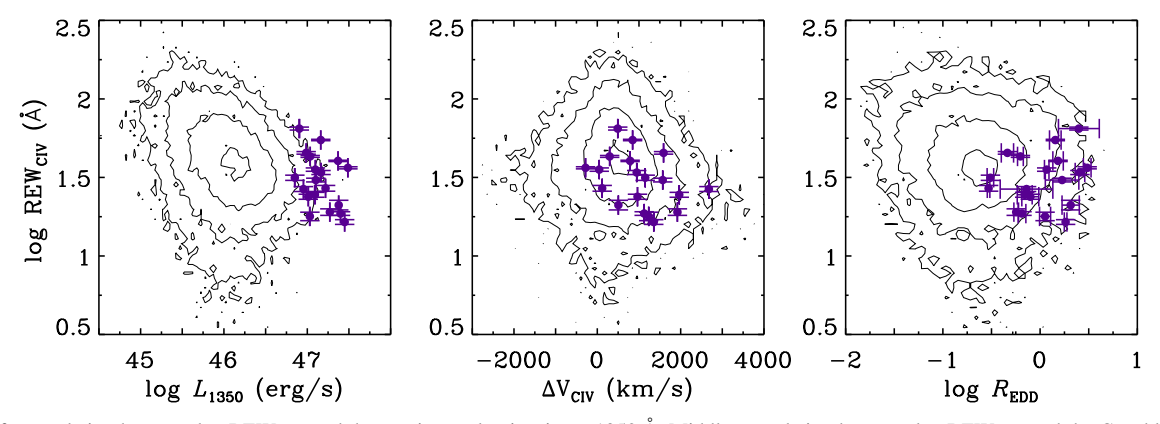


Figure 10. Left: correlation between log REW_{C IV} and the continuum luminosity at 1350 Å. Middle: correlation between log REW_{C IV} and the C IV blueshift. Right: correlation between log REW_{C IV} and log $R_{\rm EDD}$. In each panel, to show the parameter distribution of our sample with respect to the SDSS DR7 quasars, analog data from the DR7 sample of 44,424 quasars are superimposed as contours, with the border lines representing the 25th, 50th, 75th, and 95th percentile contours centered at the maximum probability point.

corrected using the accurately calculated C IV blueshifts (Allen et al. 2013; Coatman et al. 2017; Ge et al. 2019).

4.2. Baldwin Effect

The Baldwin effect is the anticorrelation between the REW values of the C IV line and the continuum luminosity at 1450 Å (Baldwin 1977). For our sample at $z \sim 3.5$, a weak anticorrelation between REW_{C IV} and the continuum luminosity at 1350 Å can be seen in the left panel of Figure 10 ($r \sim -0.31$, $p \sim 0.20$). For better comparison, in each panel, contours show the distribution of the data from the SDSS DR7 quasar sample of the 44,426 quasars as stated in Section 3.4. The absence of the Baldwin effect may be due to the narrow range of the continuum luminosity at 1350 Å in our sample ($10^{46.8} \, {\rm erg \ s^{-1}} < L_{1350} < 10^{47.8} \, {\rm erg \ s^{-1}}$), compared to that of the SDSS DR7 sample ($10^{44} \, {\rm erg \ s^{-1}} < L_{1350} < 10^{47.8} \, {\rm erg \ s^{-1}}$).

As found in previous works (Richards et al. 2002, 2011; Vietri et al. 2018), the REW_{C IV} values decrease with increasing blueshifts. Using multiepoch spectra of 362 quasars from the SDSS-RM project, Sun et al. (2018) confirmed that the extremely blueshifted quasars generally have smaller REW_{C IV}, while the reverse is not true. With the C IV blueshift range narrower than that of the quasar sample in Sun et al. (2018), we find that the REW_{C IV} values moderately anticorrelate with the C IV blueshifts with $r \sim -0.45$ ($p \sim 0.06$). The result is shown in the middle panel of Figure 10.

Some previous works proposed a modified Baldwin effect, relating REW_{C IV} and $\log R_{\rm EDD}$ (Shemmer & Lieber 2015; Ge et al. 2016). For our sample, the bolometric luminosity L_{bol} and the Eddington ratio $R_{\rm EDD}$ are directly taken from Zuo et al. (2015). The L_{bol} values are estimated with L_{5100} using the bolometric correction factor of 9.26 from the composite spectral energy distribution (SED; Richards et al. 2006), which presented that the uncertainty of the bolometric luminosity can be as much as 0.3 dex under the assumption of a single mean SED. With the bolometric luminosities and the H β -based BH masses, the $R_{\rm EDD}$ values are estimated as $L_{\rm bol}/L_{\rm EDD}$. The errors of L_{bol} and R_{EDD} listed in Table 2 of Zuo et al. (2015) only account for the statistical uncertainties estimated using the Monte Carlo approach. Including the uncertainty in the bolometric correction (~0.3 dex) and the intrinsic uncertainty of the virial BH mass estimates (~ 0.4 dex), the error propagation would yield the errors of $R_{\rm EDD}$ larger than ~ 0.5 dex.

No similar anticorrelation between the two parameters is seen in our sample, as shown in the right panel of Figure 10. We argue that it is probably due to the narrow range of $\log R_{\rm EDD}$ in our sample; the range of $\log R_{\rm EDD}$ in our sample is [-0.52, 0.49] compared to [-2, 0.5] in Ge et al. (2016) and [-2, 0.6] in the SDSS DR7 quasar sample (Shen et al. 2011). A larger sample with a wider $\log R_{\rm EDD}$ range is needed to better understand the modified Baldwin effect.

4.3. Radio Properties

To study the differences between quasars with small and large C IV blueshifts, we divide the 18 quasars with positive $\Delta V_{\rm C~IV}$ into two subsamples (subsample I and II) according to $\Delta V_{\rm C~IV}$ separated at $1000~{\rm km~s}^{-1}$; subsample II (9 quasars) has higher C IV blueshifts than that of subsample I (9 quasars).

Some previous studies showed that radio-loud quasars are strongly biased to have lower mean C IV blueshifts than the radio-quiet quasars (Marziani et al. 1996; Sulentic et al. 2007; Richards et al. 2011). As shown in Table 3, among the nine quasars in subsample I, one quasar is not in the FIRST footprint, six quasars are not detected in the FIRST, and two quasars are radio detected with the radio-loudness R as 5.5 and 2645, respectively. Among the nine quasars in subsample II, one is not in the FIRST footprint, seven are not detected in the FIRST, and one is radio detected with $R \sim 14.0$.

With a limited sample, our results show that the fraction of radio-detected quasars in subsample I is larger than that in subsample II and the loudness of the radio-loud quasar in subsample I is larger than that in subsample II. However, whether it suggests that a higher-blueshift sample is more radio-quiet still requires further verification based on a larger sample of quasars.

Using 130 low-z AGNs, Sulentic et al. (2007) found that sources with C IV blueshifts strongly favor radio-quiet Population A quasars with FWHM_{H β} \leqslant 4000 km s⁻¹ and the C IV blueshift is not observed in most Population B sources. For 0.1 < z < 3.1 and 47.4 erg s⁻¹ $< \log L_{\rm bol} < 48.4$ erg s⁻¹ AGNs, Sulentic et al. (2017) confirmed the preference of C IV blueshifts in Population A quasars and found that many Population B quasars show significant C IV blueshifts. Using the WISSH quasar sample with $L_{\rm bol} > 10^{47.3}$ erg s⁻¹, Vietri et al. (2018) also found large C IV blueshifts in sources with FWHM_{H β} > 4000 km s⁻¹.

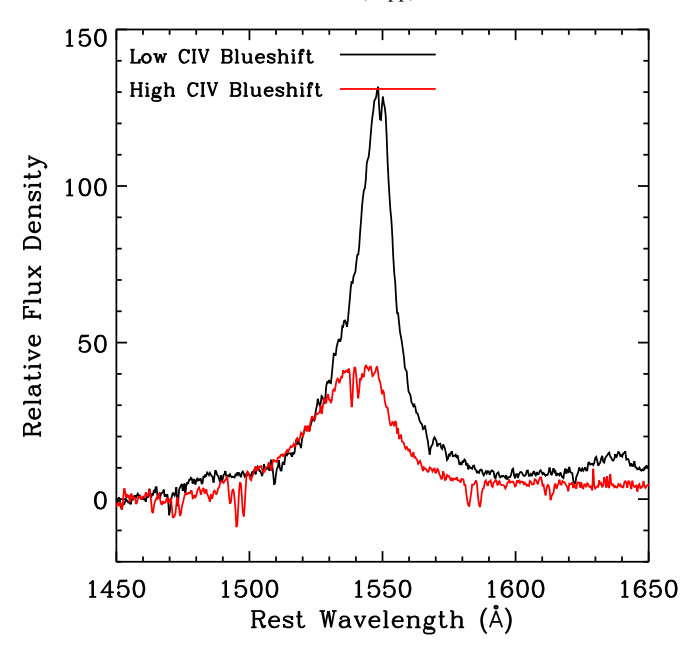


Figure 11. C IV emission lines of the composite spectra for subsamples with high and low C IV blueshifts. Black and red lines represent the composite spectra with low ($<1000~{\rm km~s}^{-1}$) and high ($>1000~{\rm km~s}^{-1}$) $\Delta V_{\rm C~IV}$ values, respectively.

Among six Population A1 quasars, only two quasars (33.3% of the Population A1 quasars) are in subsample II. Among 12 Population B quasars, 6 quasars (50% of the Population B quasars) are in subsample II with C IV blueshifts greater than $1000 \, \mathrm{km \, s^{-1}}$, extending the detection of significant C IV blueshifts in luminous Population B quasars.

4.4. Broad Emission Line Region Models

As we are more interested in the emission-line properties but not the continuum of the quasar spectra, we create two composite spectra based on the rest-frame spectra of the two subsamples using the arithmetic mean instead of the geometric mean at each wavelength pixel. After subtracting the best-fitting pseudo-continuum from the stacked spectra, we investigate their C IV emission-line profiles. As shown in Figure 11, the blue wings are similar, while the red wing of the C IV line profile with larger blueshift is lower. It appears that the shift of the C IV emission line is not due to the blueshift of the whole profile but to the suppression of the red wing.

Richards et al. (2002) suggested that the C IV blueshifts were related to the quasar orientation, either external or internal. In a spherically symmetric cloud model (Elvis 2000; Richards et al. 2002), assuming that the outflowing clouds are isotropically distributed, subsample I may represent a more face-on configuration of the accretion disk, and subsample II represents a more edge-on configuration (Richards et al. 2002; Leighly 2004; Coatman et al. 2017, 2016). The obscuration of the optically thick disk in subsample II would reduce the flux of the red wing of C IV, whereas for a disk-wind-type model (Murray & Chiang 1998), the blueshift and shape could be caused by both the orientation and a change in the opening angle of the disk wind.

However, Leighly (2004) and Richards et al. (2011) hinted that the C IV blueshifts are not likely due to the external orientation. Leighly (2004) mentioned that the blueshifted

high-ionization lines may come from a wind that is moving toward us, with the receding side obscured by the optically thick accretion disk. Moreover, some studies suggested that the blueshift implied the contribution from the outflowing wind component (Bachev et al. 2004; Marziani et al. 2010, 2019; Richards et al. 2011; Vietri et al. 2018).

In that way, the differences of the C IV properties between subsamples I and II are due to differences in the accretion disk wind, where the relative contribution of the wind component to the disk contribution in subsample II is larger. Furthermore, the difference of the disk wind is probably due to the difference of the SED, ultimately determined by the intrinsic quasar properties, such as the Eddington ratio (Richards et al. 2011; Sulentic et al. 2017; Sun et al. 2018; Vietri et al. 2018; Marziani et al. 2019).

On the other hand, we compared the REW_[O III] distribution of the two subsamples. We find that depending on REW_[O III] > 5 or <5 Å (Vietri et al. 2018), subsample I can be divided into six [O III] and three weak [O III] quasars, while subsample II contains one [O III] quasars and eight weak [O III] quasars. The higher ratio of [O III] quasars in subsample I with lower blueshifts suggests that the [O III] quasars seem to exhibit lower blueshifts than the weak [O III] quasars. This is qualitatively consistent with the result found in Vietri et al. (2018), where among 18 quasars with 2 < z < 4 and $L_{\rm bol} > 10^{47.3}\,{\rm erg\,s^{-1}}$, the 6 [O III] quasars show lower blueshifts than the other 12 weak [O III] quasars.

Shen & Ho (2014) suggested that the dispersion of the FWHM_{H β} at fixed $R_{\text{Fe II}}$ in the optical EV1 plane is largely an orientation effect and found no tendency of the REW_[O III] values with FWHM_{H β} at fixed $R_{\text{Fe II}}$. That indicates that the REW_[O III] distribution cannot be solely explained by the orientation effect.

Since the 18 quasars of our sample exhibit $R_{\rm Fe\ II}$ values ranging from 0 to 0.47, as shown in Figure 9, it is reasonable to assume that they are quasars with almost fixed $R_{\rm Fe\ II}$ and to take the FWHM_{H β} as an orientation indicator. No significant correlations between FWHM_{H β} and the C IV blueshifts and REW_[O III] are found, with $r\sim 0.25$ ($p\sim 0.32$) and $r\sim 0.09$ ($p\sim 0.73$), respectively. It indicates that neither the C IV blueshifts nor the distribution of REW_[O III] would be likely explained by the orientation effect alone.

Though our results cannot help constrain the details of the broad emission line region models, the strongly blueshifted C IV line profile suggests that it is at least partly contributed by the emission in the wind. The possibility of an orientation effect cannot be neglected, but the orientation effect alone is unlikely to explain either the C IV blueshift or the REW $_{\rm [O\ III]}$ distribution. It is possible that they are caused by the combination of the orientation effect and the intrinsic quasar properties, such as the Eddington ratio.

4.5. Is the C IV Blueshift Driven by the Eddington Ratio?

As shown in Figure 12, adopting $R_{\rm EDD}$ estimated from the H β -based BH masses, all the quasars in our sample are accreting at $R_{\rm EDD} > 0.30$ and cover a considerable range of blueshifts. It suggests that not all quasars with high Eddington ratios show large blueshifts. This is consistent with previous works (Baskin & Laor 2005; Coatman et al. 2016; Sun et al. 2018), where quasars with large C IV blueshifts tend to accrete at around Eddington limits, while the converse is not true.

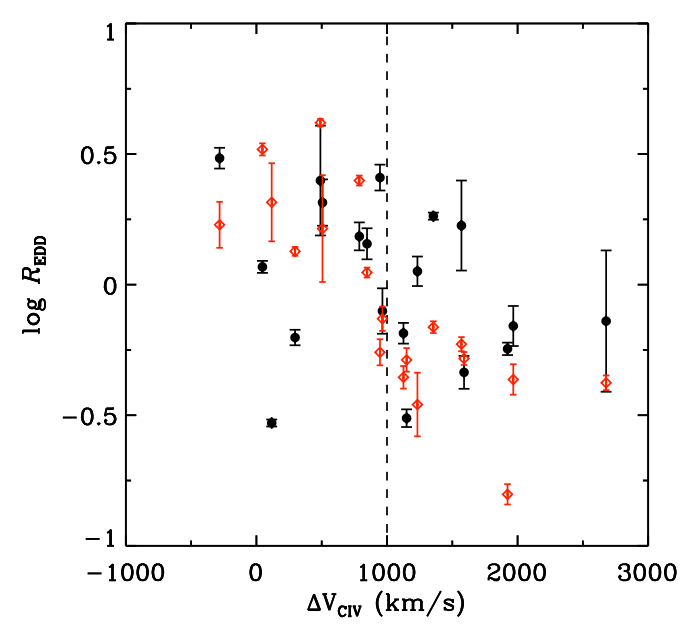


Figure 12. Eddington ratio vs. the C IV blueshift, where the black and red symbols refer to the H β -based log $R_{\rm EDD}$ and the C IV-based log $R_{\rm EDD}$ values, respectively. The quasars in our sample are accreting at $R_{\rm EDD}>0.3$ and cover a large range of blueshifts.

The Eddington ratio is thought to be the underlying driver behind the MS (Boroson & Green 1992; Sulentic et al. 2000, 2017; Marziani et al. 2001; Bachev et al. 2004; Marziani et al. 2010, 2019; Shen & Ho 2014). As the $R_{\rm EDD}$ value increases, the radiation pressure plays an increasingly important role in accelerating clouds that could produce a blueshifted C IV profile (Marziani et al. 2010). Previous studies found that there is a correlation between the C IV line blueshifts and the $R_{\rm EDD}$ values (Marziani et al. 2010; Coatman et al. 2016; Sun et al. 2018; Vietri et al. 2018).

No similar correlation between the C IV blueshifts and $R_{\rm EDD}$ is seen in our sample, with $r \sim -0.2$ ($p \sim 0.4$). The median $\log R_{\rm EDD}$ of the quasars in subsample I is 0.16 \pm 0.42, while that of the quasars in subsample II is -0.16 ± 0.30 . The scatter is estimated as the inner 50th percentile of the distribution. From the difference of the median $\log R_{\rm EDD}$, it seems that the quasars of subsample I accrete at higher Eddington ratio than the quasars of subsample II. However, this may not be representative of the intrinsic relationship, as both the errors of $R_{\rm EDD}$ (~ 0.5 dex) and the scatters of the median $\log R_{\rm EDD}$ are large compared to the difference of the median $\log R_{\rm EDD}$ between subsamples I and II. If the $R_{\rm EDD}$ values are estimated from the C_{IV}-based BH masses, as shown in red, an anticorrelation between the C IV line blueshifts and the $R_{\rm EDD}$ is shown, with $r \sim -0.86$ (p < 0.01). This anticorrelation is mainly due to the positive correlation between the C IV line blueshifts and the CIV-based BH masses, as shown in Section 3.2.

In the optical EV1 plane, the average $R_{\rm EDD}$ value increases as the $R_{\rm Fe~II}$ increases (Shen & Ho 2014; Marziani et al. 2019). Our sample including only the Population A1 and Population B quasars with $R_{\rm Fe~II} < 0.5$ covers the left part in the optical EV1 plane. Thus, we argue that the inconsistent correlation between the C IV blueshifts and $R_{\rm EDD}$ in our sample is mainly due to the limited sample size and the range of the $R_{\rm EDD}$, which should be verified with a larger sample in the future.

5. Conclusion

Using a $z \sim 3.5$ luminous quasar sample ($10^{47.5}$ erg s⁻¹ < $L_{\rm bol} < 10^{48.3}\,{\rm erg\,s^{-1}}$) with observed-frame optical and NIR spectroscopy, we have investigated the reliability of estimating BH masses based on the C IV emission line and the possible corrections based on the C IV blueshift and asymmetry. We also study the C IV emission-line properties, in terms of the blueshift and possible physical mechanisms therein. The conclusions are summarized as follows:

- 1. The logarithms of the C IV-to-H β BH mass ratios are between -0.85 and 0.67 dex, with a median value as 0.110 dex and a scatter as 0.647 dex. A total of 63% of quasars in our sample show $\log M_{\rm BH}({\rm C\,IV})/M_{\rm BH}({\rm H}\beta)$ within the range of 0.4 dex. This suggests that the C IV-based BH mass estimates still need to be corrected to better match the H β -based BH masses.
- 2. The logarithms of the C IV-to-H β BH mass ratios correlate with the C IV FWHMs, the C IV blueshifts, and the asymmetries. Corrections using the C IV blueshift and the asymmetry reduce the scatter of the logarithm of the mass ratio by \sim 0.2 and \sim 0.04 dex, respectively. Excluding the target with the largest C IV-to-H β mass difference, the scatter is reduced by \sim 0.3 dex after the correction using the C IV asymmetry.
- 3. The Baldwin effect between $REW_{C\,IV}$ and $\log L_{1350}$ is not significant in our sample, likely due to the limited luminosity range of our sample. The moderate anticorrelation between $REW_{C\,IV}$ and the C IV blueshifts is seen. No similar anticorrelation between $REW_{C\,IV}$ and R_{EDD} (the modified Baldwin effect) is seen, which may be mainly due to the narrow range of $\log R_{EDD}$ of our sample.
- 4.With a limited number of quasars, we find that in subsample I with positive C IV blueshifts $< 1000 \,\mathrm{km\,s}^{-1}$ among the eight quasars in the FIRST footprint, two quasars are radio detected, including one radio-loud quasar with $R \sim 2645$ and one radio-quiet quasar with $R \sim 5.5$, while in subsample II among the eight quasars in the FIRST footprint, one quasar is radio detected in the FIRST with $R \sim 14.0$. Whether it suggests that a higher blueshift sample is more radio-quiet still needs to be verified using a larger quasar sample in the future.
- 5. Among the 19 quasars, six are Population A1 and 12 are Population B. A total of 50% of the Population B quasars exhibit C IV blueshifts larger than 1000 km s⁻¹, extending the detection of significant C IV blueshifts in luminous Population B quasars.
- 6. After comparing the C IV emission-line profiles of the composite spectra of subsamples I and II, we find a lack of flux in the red wing for the C IV composite emission line of subsample II with larger blueshifts. The ratio of [O III] quasars with REW $_{\rm [O~III]} > 5$ Å in subsample I is higher by 55.6% than that in subsample II, suggesting that the [O III] quasars seem to exhibit lower blueshifts than the weak [O III] quasars with REW $_{\rm [O~III]} < 5$ Å.
- 7. Considering that our sample mainly covers a narrow range of $R_{\rm Fe\ II} < 0.5$, we take the FWHM_{H β} as an indicator of the orientation. No significant correlation between FWHM_{H β} and the C IV blueshifts or REW_[O III] is found, indicating that the orientation effect alone cannot explain either the difference of the C IV profile for quasars with different blueshifts or the distribution of REW_[O III]. It is more likely that they are caused by the orientation effect and the intrinsic quasar properties, such as the Eddington ratio.
- 8. Quasars in our sample accrete at high Eddington ratios with $R_{\rm EDD} > 0.3$ and show a wide range of C IV blueshifts,

with 18/19 of the quasars showing C IV blueshifts (with the median value of 1126 km s⁻¹) and 14/19 of the quasars showing C IV blueshifts larger than 500 km s⁻¹.

We thank the anonymous referee for the helpful comments that improved the paper. We thank the National Key R&D Program of China (2016YFA0400703) and the National Science Foundation of China (11533001, 11721303) for support. This work made use of the facilities of the Center for High Performance Computing at Shanghai Astronomical Observatory, Chinese Academy of Sciences. This research uses data obtained through the Telescope Access Program (TAP), which is funded by the National Astronomical Observatories, Chinese Academy of Sciences, and the Special Fund for Astronomy from the Ministry of Finance. Observations obtained with the Hale Telescope at Palomar Observatory were obtained as part of an agreement between the National Astronomical Observatories, Chinese Academy of Sciences, and the California Institute of Technology. The LBT is an international collaboration among institutions in the United States, Italy, and Germany. LBT Corporation partners are as follows: the University of Arizona on behalf of the Arizona university system; Istituto Nazionale di Astrofisica, Italy; LBT Beteiligungsgesellschaft, Germany, representing the Max-Planck Society, the Astrophysical Institute Potsdam, and Heidelberg University; The Ohio State University; and the Research Corporation, on behalf of the University of Notre Dame, University of Minnesota, and University of Virginia. Funding for the SDSS and SDSS-II has been provided by the Alfred P. Sloan Foundation, the Participating Institutions, the National Science Foundation, the U.S. Department of Energy, the National Aeronautics and Space Administration, the Japanese Monbukagakusho, the Max Planck Society, and the Higher Education Funding Council for England. The SDSS website is http://www.sdss.org/. The SDSS is managed by the Astrophysical Research Consortium for the Participating Institutions. The Participating Institutions are the American Museum of Natural History, Astrophysical Institute Potsdam, University of Basel, University of Cambridge, Case Western Reserve University, University of Chicago, Drexel University, Fermilab, the Institute for Advanced Study, the Japan Participation Group, Johns Hopkins University, the Joint Institute for Nuclear Astrophysics, the Kavli Institute for Particle Astrophysics and Cosmology, the Korean Scientist Group, the Chinese Academy of Sciences (LAMOST), Los Alamos National Laboratory, the Max-Planck-Institute for Astronomy (MPIA), the Max-Planck Institute for Astrophysics (MPA), New Mexico State University, Ohio State University, University of Pittsburgh, University of Portsmouth, Princeton University, the United States Naval Observatory, and the University of Washington.

Appendix

In Model A, we fit three Gaussians for the BC of C IV, one Gaussian for the BC of He II $\lambda 1640$, and one Gaussian for the BC of O III] $\lambda 1663$. In model B, we fit 2/1 Gaussians for the BC/NC of C IV, 1/1 Gaussian for the BC/NC of He II, and 1/1 Gaussian for the BC/NC of O III]. The NCs of the three lines are tied together and fitted with an upper FWHM limit as $1600~{\rm km\,s^{-1}}$. We also compare them with Model C, where the only difference from Model A is that the number of Gaussians used to fit the C IV BC in Model C is 2 instead of 3.

Figures A1 and A2 present the spectra fitting results of Model A and Model B in the wavelength range of 1500–1700 Å for the 19 quasars, respectively. The reduced χ^2 of the spectral fitting of the C IV emission line using Models A, B, and C are listed in Table A1, with the median values as 1.07 ± 0.25 , 1.06 ± 0.27 , and 1.16 ± 0.34 , respectively. Model A yields the smallest χ^2 for 68.4% quasars, though considering the scatter, the χ^2 values of the three models are similar.

However, after visual inspections, we find that for most quasars the three-Gaussian models (Model A and B) for the C IV line reproduce the C IV line profile better than the two-Gaussian model (Model C). This is reasonable, as there are more adjustable parameters to maximize the consistency between the model fitting and the observed data. For some quasars, such as J011521.20+152453.3 and J014214.75+002324.2, the fitting results from Model B show a weird NC owing to the narrow spikes in the noisy regions of the spectra.

If the candidate model selected from the visual inspection (as listed in Column (7) of Table A1) is different from the the best model according to the χ^2 comparison (as listed in Column (6)), we adopt the candidate model from the visual inspection. If both Model A and Model B are listed in Columns (6) and (7), we adopt the results from Model A, which is supported by the Akaike information criterion (AIC) comparison, as listed in Column (5).

To determine the best model for the data, we derive the AIC values of Model A and Model B for each object. The optimal choice is the one with the smaller AIC value. The AIC is calculated as

$$AIC = -2\log L(\hat{\theta}) + 2k, \tag{A1}$$

where θ is the set of model parameters, k is the number of the independently adjusted parameters in the candidate model, and $L(\hat{\theta})$ is the likelihood of the candidate model giving the data when evaluated at the maximum likelihood estimate of θ (Akaike 1974). The derived AIC values from Model A and Model B are listed in Table A1, showing that Model A is better to approximate the data than Model B.

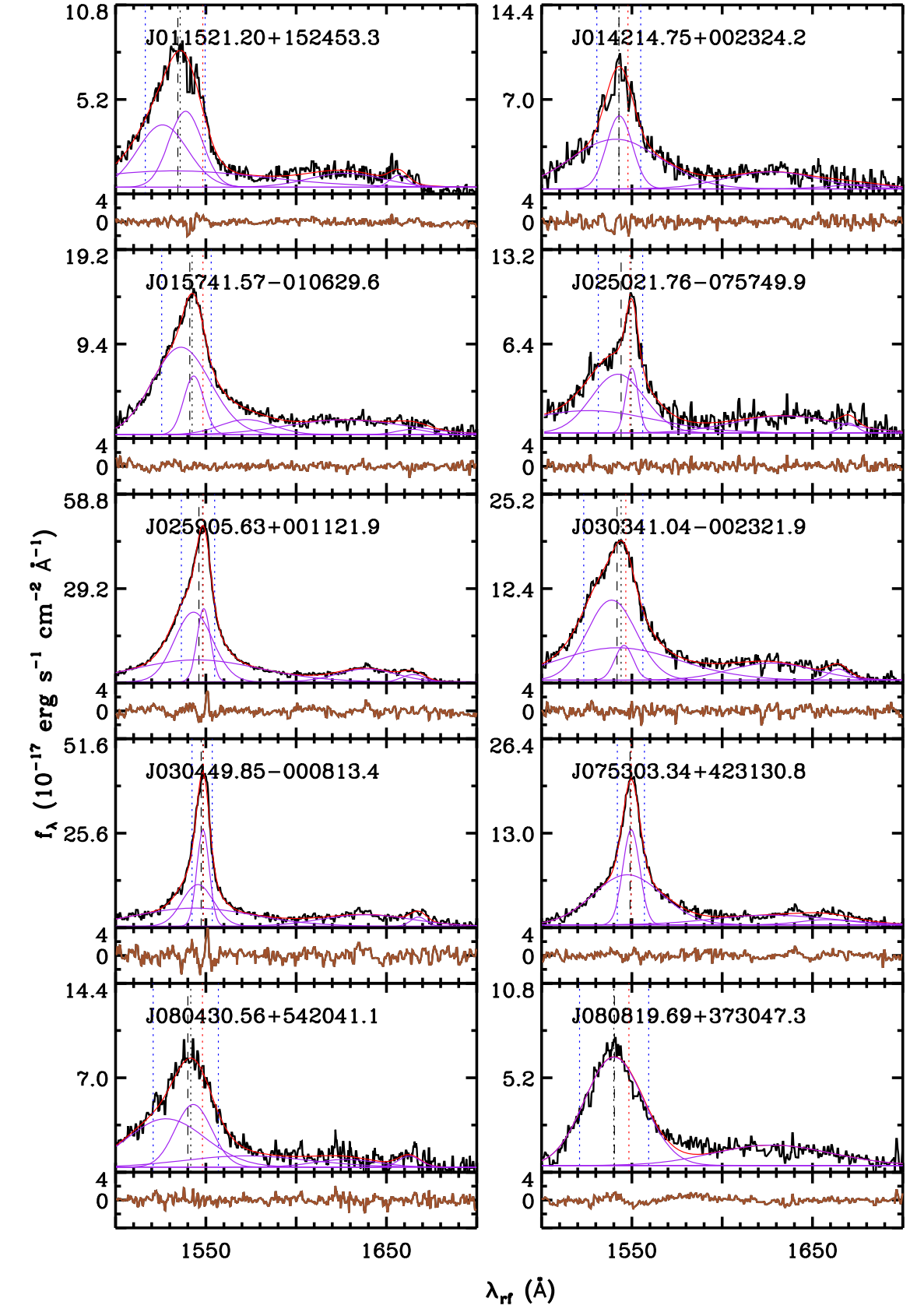


Figure A1. Fitting results of the C IV line complex in the wavelength range of 1500–1700 Å for the 19 quasars using Model A, where the spectrum in each panel is shown in black, the combined model fitting is shown in red, the individual Gaussian for the BC is shown in purple, and the fitting residuals are shown in brown. The vertical blue dashed lines from left to right refer to the wavelengths of λ_{blue} and λ_{red} . The vertical red dashed line refers to the wavelength of λ_{lab} . The vertical black dashed and long-dashed lines refer to the wavelength of λ_0 and λ_{half} , respectively.

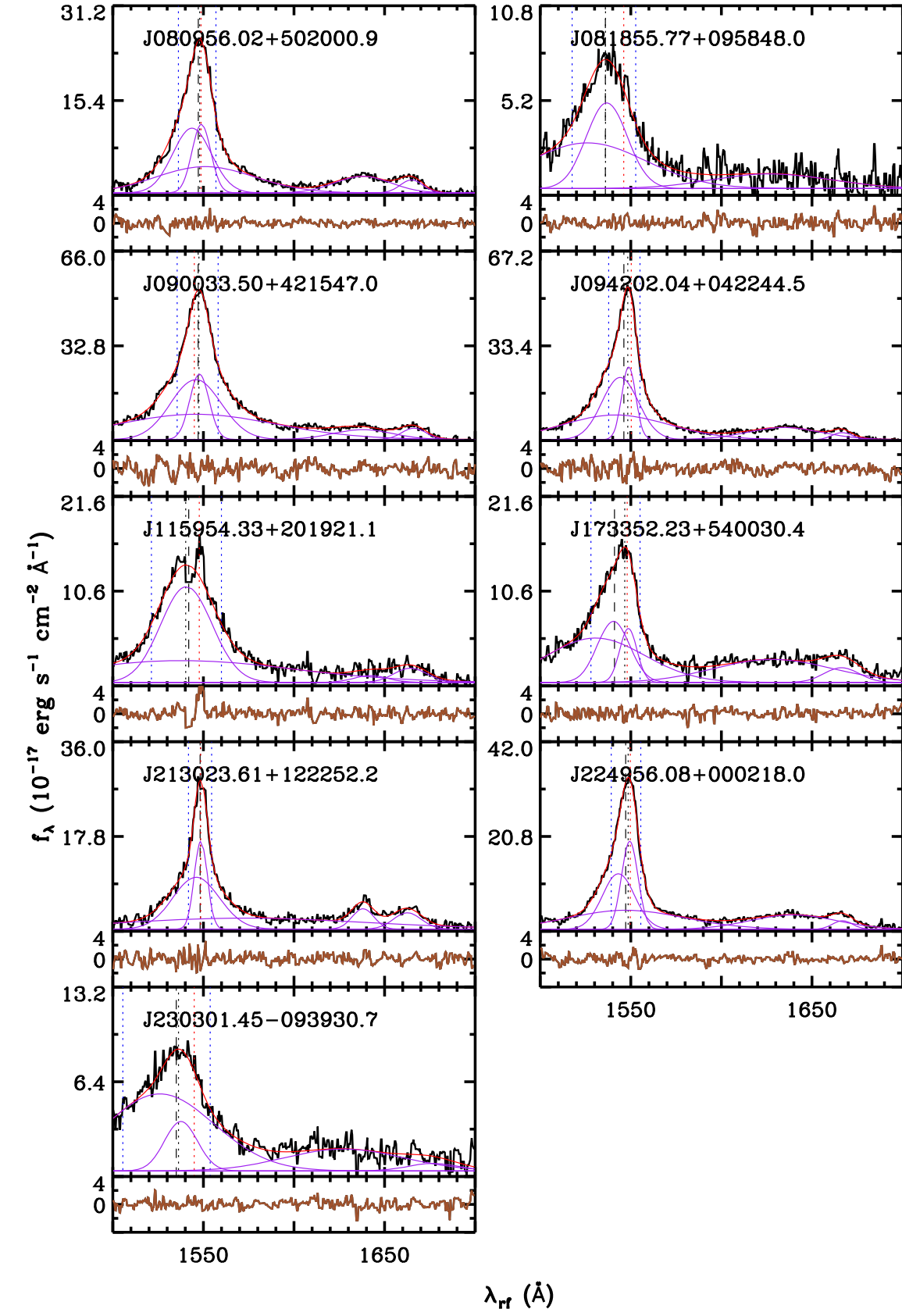


Figure A1. (Continued.)

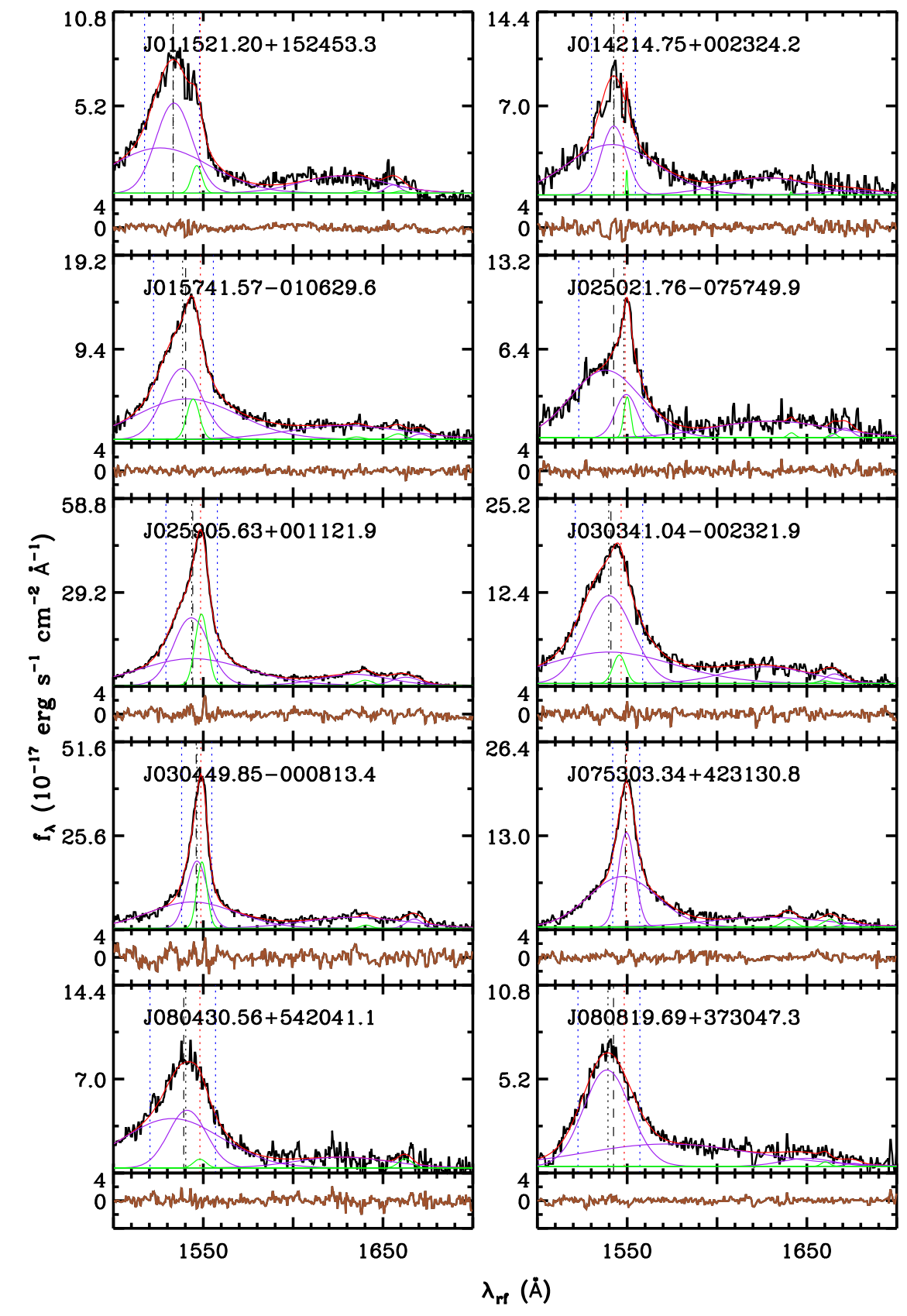


Figure A2. Fitting results of the C IV line complex in the wavelength range of 1500–1700 Å for the 19 quasars using Model B, where the spectrum in each panel is shown in black, the combined model fitting is shown in red, the individual Gaussian for the BC is shown in purple, the individual Gaussian for the NC is shown in green, and the fitting residuals are shown in brown. The vertical blue dashed lines from left to right refer to the wavelengths of λ_{blue} and λ_{red} . The vertical red dashed line refers to the wavelength of λ_{lab} . The vertical black dashed and long-dashed lines refer to the wavelength of λ_{0} and λ_{half} , respectively.

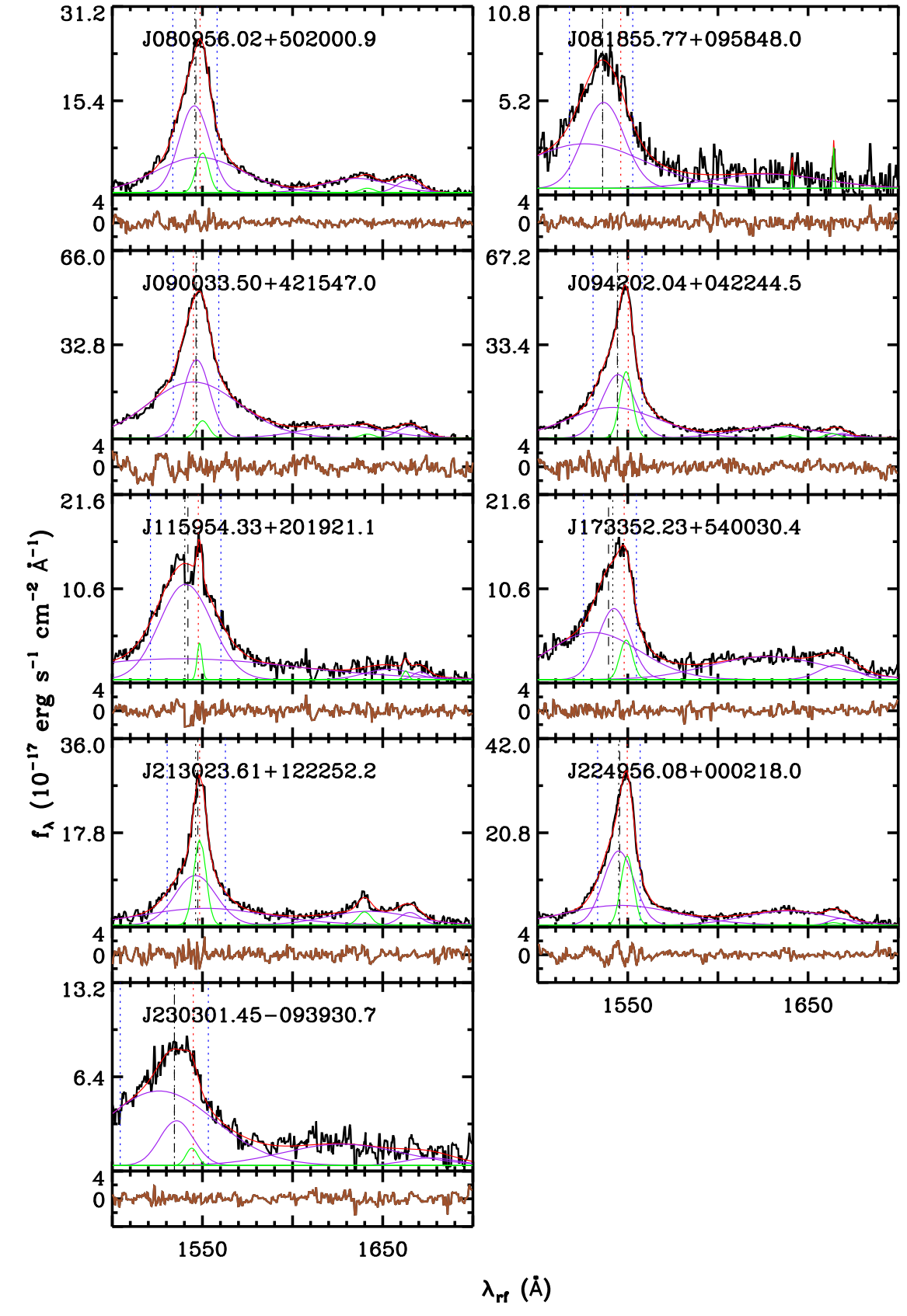


Figure A2. (Continued.)

Table A1The Fitting Details of the C IV Emission Line

Name (SDSS)	χ^2	χ^2	χ^2	AIC_A - AIC_B	χ^2	Visual	Final
	A	В	C		Comparison	Inspection	
(1)	(2)	(3)	(4)	(5)	(6)	(7)	(8)
J011521.20+152453.3	1.29	1.30	1.34	-4.001	A	A	A
J014214.75+002324.2	1.21	1.20	1.24	-4.004	В	A	A
J015741.57-010629.6	0.96	0.88	1.08	-3.998	В	В	В
J025021.76-075749.9	0.96	0.96	0.98	-3.999	AB	В	В
J025905.63+001121.9	1.02	1.00	2.18	-4.000	В	AB	В
J030341.04-002321.9	0.97	1.00	1.07	-4.001	A	A	A
J030449.85-000813.4	0.90	0.93	1.00	-4.000	A	В	В
J075303.34+423130.8	1.97	1.88	1.89	-3.998	В	AB	В
J080430.56+542041.1	1.16	1.18	1.16	-4.003	A	A	A
J080819.69+373047.3	1.09	0.89	0.87	-3.984	В	В	В
J080956.02+502000.9	1.01	1.06	1.23	-4.001	A	A	A
J081855.77+095848.0	1.17	1.19	1.16	-3.998	A	A	A
J090033.50+421547.0	1.07	1.11	1.12	-4.001	A	В	В
J094202.04+042244.5	1.00	1.00	1.39	-4.000	AB	AB	A
J115954.33+201921.1	1.11	1.10	1.18	-3.997	В	A	A
J173352.23+540030.4	0.85	0.85	0.90	-4.000	AB	AB	A
J213023.61+122252.0	1.22	1.24	1.28	-4.001	A	AB	A
J224956.08+000218.0	1.35	1.39	1.92	-4.001	A	A	A
J230301.45-093930.7	0.89	0.90	0.90	-4.002	A	A	A

Note. Column (1): name of the quasars. Column (2): reduced χ^2 of the spectral fitting to the C IV line complex using Model A. Column (3): reduced χ^2 of the spectral fitting to the C IV line complex using Model C. Column (5); difference of the AIC values between Model A and Model B. Column (6): preferred model with the lower reduced χ^2 between Model A and Model B. Column (7): preferred model from the visual inspection between Model A and Model B. Column (8): final adopted model from the combination of the results from Columns (5)–(7).

In all, for seven quasars (J015741.57–010629.6, J025021.76–075749.9, J025905.63+001121.9, J030449.85–000813.4, J075 303.34+423130.8, J080819.69+373047.3, and J090033.50+421 547.0), small fitting residuals around the C IV line are seen in the results from Model A but not shown in the results from Model B. Therefore, for these seven quasars we use the results from Model B, and for the other 12 quasars we adopt the results from Model A.

ORCID iDs

Wenwen Zuo https://orcid.org/0000-0002-4521-6281 Xue-Bing Wu https://orcid.org/0000-0002-7350-6913 Xiaohui Fan https://orcid.org/0000-0003-3310-0131 Richard Green https://orcid.org/0000-0003-1245-5232 Weimin Yi https://orcid.org/0000-0001-9314-0552 Andreas Schulze https://orcid.org/0000-0002-6660-6131 Ran Wang https://orcid.org/0000-0003-4956-5742 Fuyan Bian https://orcid.org/0000-0002-1620-0897

References

```
Akaike, H. 1974, ITAC, 19, 716
Akritas, M. G., & Bershady, M. A. 1996, ApJ, 470, 706
Allen, J. T., Hewett, P. C., Richardson, C. T., Ferland, G. J., & Baldwin, J. A. 2013, MNRAS, 430, 3510
Assef, R. J., Denney, K. D., Kochanek, C. S., et al. 2011, ApJ, 742, 93
Bachev, R., Marziani, P., Sulentic, J. W., et al. 2004, ApJ, 617, 171
Baldwin, J. A. 1977, ApJ, 214, 679
Barth, A. J., Bennert, V. N., Canalizo, G., et al. 2015, ApJS, 217, 26
Baskin, A., & Laor, A. 2005, MNRAS, 356, 1029
Becker, G. D., Rauch, M., & Sargent, W. L. W. 2009, ApJ, 698, 1010
Bentz, M. C., Denney, K. D., Grier, C. J., et al. 2013, ApJ, 767, 149
Bentz, M. C., Peterson, B. M., Netzer, H., Pogge, R. W., & Vestergaard, M. 2009, ApJ, 697, 160
Bian, F., Fan, X., Bechtold, J., et al. 2010, ApJ, 725, 1877
Boroson, T. A., & Green, R. F. 1992, ApJS, 80, 109
```

```
Cardelli, J. A., Clayton, G. C., & Mathis, J. S. 1989, ApJ, 345, 245
Coatman, L., Hewett, P. C., Banerji, M., et al. 2017, MNRAS, 465, 2120
Coatman, L., Hewett, P. C., Banerji, M., & Richards, G. T. 2016, MNRAS,
  461, 647
Coffey, D., Salvato, M., Merloni, A., et al. 2019, A&A, 625, A123
Cushing, M. C., Vacca, W. D., & Rayner, J. T. 2004, PASP, 116, 362
Denney, K. D. 2012, ApJ, 759, 44
Denney, K. D., Peterson, B. M., Pogge, R. W., et al. 2010, ApJ, 721, 715
Du, P., Hu, C., Lu, K.-X., et al. 2014, ApJ, 782, 45
Elvis, M. 2000, ApJ, 545, 63
Feibelman, W. A. 1983, A&A, 122, 335
Ferrarese, L., & Merritt, D. 2000, ApJL, 539, L9
Gaskell, C. M. 1982, ApJ, 263, 79
Ge, X., Bian, W.-H., Jiang, X.-L., Liu, W.-S., & Wang, X.-F. 2016, MNRAS,
Ge, X., Zhao, B.-X., Bian, W.-H., & Frederick, G. R. 2019, AJ, 157, 148
Gebhardt, K., Bender, R., Bower, G., et al. 2000, ApJL, 539, L13
Graham, A. W., Onken, C. A., Athanassoula, E., & Combes, F. 2011,
  MNRAS, 412, 2211
Greene, J. E., & Ho, L. C. 2005, ApJ, 630, 122
Greene, J. E., Peng, C. Y., & Ludwig, R. R. 2010, ApJ, 709, 937
Grier, C. J., Shen, Y., Horne, K., et al. 2019, ApJ, 887, 38
Grier, C. J., Trump, J. R., Shen, Y., et al. 2017, ApJ, 851, 21
Gültekin, K., Richstone, D. O., Gebhardt, K., et al. 2009, ApJ, 698, 198
Herter, T. L., Henderson, C. P., Wilson, J. C., et al. 2008, Proc. SPIE, 7014,
  70140X
Hill, J. M., Green, R. F., Ashby, D. S., et al. 2012, Proc. SPIE, 8444, 84441A
Jiang, L., Fan, X., Ivezić, Ž., et al. 2007, ApJ, 656, 680
Kaspi, S., Brandt, W. N., Maoz, D., et al. 2007, ApJ, 659, 997
Kaspi, S., Maoz, D., Netzer, H., et al. 2005, ApJ, 629, 61
Kaspi, S., Smith, P. S., Netzer, H., et al. 2000, ApJ, 533, 631
Kelly, B. C. 2007, ApJ, 665, 1489
Konigl, A., & Kartje, J. F. 1994, ApJ, 434, 446
Kormendy, J., & Ho, L. C. 2013, ARA&A, 51, 511
Leighly, K. M. 2004, ApJ, 611, 125
MacLeod, C. L., Ivezić, Ž, Sesar, B., et al. 2012, ApJ, 753, 106
Marziani, P., Calvani, M., & Braito, V. 2001, MmSAI, 72, 41
Marziani, P., del Olmo, A., Martínez-Carballo, M. A., et al. 2019, A&A,
  627, A88
Marziani, P., Sulentic, J. W., Dultzin-Hacyan, D., Calvani, M., & Moles, M.
   1996, ApJS, 104, 37
```

```
Marziani, P., Sulentic, J. W., Negrete, C. A., et al. 2010, MNRAS, 409, 1033
Marziani, P., Zamanov, R. K., Sulentic, J. W., & Calvani, M. 2003, MNRAS,
   345, 1133
McGill, K. L., Woo, J.-H., Treu, T., & Malkan, M. A. 2008, ApJ, 673, 703
McLure, R. J., & Jarvis, M. J. 2002, MNRAS, 337, 109
Mejía-Restrepo, J. E., Trakhtenbrot, B., Lira, P., & Netzer, H. 2018, MNRAS,
   478, 1929
Murray, N., & Chiang, J. 1998, ApJ, 494, 125
Murray, N., Chiang, J., Grossman, S. A., & Voit, G. M. 1995, ApJ, 451, 498
Nelson, C. H., Green, R. F., Bower, G., Gebhardt, K., & Weistrop, D. 2004,
Onken, C. A., Ferrarese, L., Merritt, D., et al. 2004, ApJ, 615, 645
Park, D., Barth, A. J., Woo, J.-H., et al. 2017, ApJ, 839, 93
Park, D., Woo, J.-H., Denney, K. D., & Shin, J. 2013, ApJ, 770, 87
Peterson, B. M. 1993, PASP, 105, 247
Peterson, B. M., Ferrarese, L., Gilbert, K. M., et al. 2004, ApJ, 613, 682
Proga, D., Stone, J. M., & Kallman, T. R. 2000, ApJ, 543, 686
Richards, G. T., Kruczek, N. E., Gallagher, S. C., et al. 2011, AJ, 141, 167
Richards, G. T., Lacy, M., Storrie-Lombardi, L. J., et al. 2006, ApJS, 166, 470
Richards, G. T., Vanden Berk, D. E., Reichard, T. A., et al. 2002, AJ, 124, 1
Runnoe, J. C., Brotherton, M. S., Shang, Z., & DiPompeo, M. A. 2013,
   MNRAS, 434, 848
Schlegel, D. J., Finkbeiner, D. P., & Davis, M. 1998, ApJ, 500, 525
Schneider, D. P., Richards, G. T., Hall, P. B., et al. 2010, AJ, 139, 2360
```

Schulze, A., Silverman, J. D., Kashino, D., et al. 2018, ApJS, 239, 22

```
Shemmer, O., & Lieber, S. 2015, ApJ, 805, 124
Shen, Y. 2013, BASI, 41, 61
Shen, Y., Brandt, W. N., Dawson, K. S., et al. 2015, ApJS, 216, 4
Shen, Y., Greene, J. E., Strauss, M. A., Richards, G. T., & Schneider, D. P.
  2008, ApJ, 680, 169
Shen, Y., Grier, C. J., Horne, K., et al. 2019, ApJL, 883, L14
Shen, Y., & Ho, L. C. 2014, Natur, 513, 210
Shen, Y., & Liu, X. 2012, ApJ, 753, 125
Shen, Y., Richards, G. T., Strauss, M. A., et al. 2011, ApJS, 194, 45
Sulentic, J. W., Bachev, R., Marziani, P., Negrete, C. A., & Dultzin, D. 2007,
    ApJ, 666, 757
Sulentic, J. W., del Olmo, A., Marziani, P., et al. 2017, A&A, 608, A122
Sulentic, J. W., Marziani, P., & Dultzin-Hacyan, D. 2000, ARA&A, 38, 521
Sun, M., Xue, Y., Richards, G. T., et al. 2018, ApJ, 854, 128
Trakhtenbrot, B., & Netzer, H. 2012, MNRAS, 427, 3081
Tremaine, S., Gebhardt, K., Bender, R., et al. 2002, ApJ, 574, 740
Vanden Berk, D. E., Richards, G. T., Bauer, A., et al. 2001, AJ, 122, 549
Vestergaard, M. 2002, ApJ, 571, 733
Vestergaard, M., & Osmer, P. S. 2009, ApJ, 699, 800
Vestergaard, M., & Peterson, B. M. 2006, ApJ, 641, 689
Vietri, G., Piconcelli, E., Bischetti, M., et al. 2018, A&A, 617, A81
Wilhite, B. C., Brunner, R. J., Schneider, D. P., & Vanden Berk, D. E. 2007,
  ApJ, 669, 791
Zuo, W., Wu, X.-B., Fan, X., et al. 2015, ApJ, 799, 189
Zuo, W., Wu, X.-B., Liu, Y.-Q., & Jiao, C.-L. 2012, ApJ, 758, 104
```